Title:

Histone demethylase KDM6A directly senses oxygen to control chromatin and cell fate

Authors: Abhishek A. Chakraborty[1], Tuomas Laukka[2], Matti Myllykoski[2], Alison E. Ringel[3], Matthew A. Booker[4], Michael Y. Tolstorukov[4], Yuzhong Jeff Meng[1,5,6,7,8], Samuel R. Meier[5], Rebecca B. Jennings[9], Amanda L. Creech[5], Zachary T. Herbert [10], Samuel K. McBrayer[1], Benjamin A. Olenchock[11], Jacob D. Jaffe[5], Marcia C. Haigis[3], Rameen Beroukhim[1,5,7], Sabina Signoretti[9], Peppi Koivunen[2, *], and William G. Kaelin, Jr.[1,12,*]

Affiliations:

[1]Department of Medical Oncology, Dana-Farber Cancer Institute and Brigham and Women's Hospital, Harvard Medical School, Boston, MA 02215, USA.

[2]Biocenter Oulu, Faculty of Biochemistry and Molecular Medicine, Oulu Center for Cell-Matrix Research, University of Oulu, FIN-90014 Oulu, Finland.

[3]Department of Cell Biology, Harvard Medical School, Boston, MA 02115, USA.

[4]Department of Informatics, Dana-Farber Cancer Institute, Harvard Medical School, Boston, MA 02215, USA.

[5]Broad Institute of Harvard and MIT, Cambridge, MA 02142, USA.

[6]Biological and Biomedical Sciences, Harvard Medical School, Boston, MA 02115, USA.

[7]Department of Cancer Biology, Dana-Farber Cancer Institute, Boston, MA, Harvard Medical School, Boston, MA 02115, USA.

[8]The Harvard-MIT Program in Health Sciences and Technology, Harvard Medical School, Boston, MA

[9]Department of Pathology, Brigham and Women's Hospital, Harvard Medical School, Boston, MA 02115, USA

[10]Molecular Biology Core Facility, Dana-Farber Cancer Institute and Brigham and Women's Hospital, Harvard Medical School, Boston, MA 02215, USA.

[11]Division of Cardiovascular Medicine, Department of Medicine, The Brigham and Women's Hospital, Boston, MA 02115, USA; Harvard Medical School, Boston, MA 02115, USA.

[12]Howard Hughes Medical Institute, Chevy Chase, MD 20815, USA.

*Corresponding author. Email: william_kaelin@dfci.harvard.edu (W.G.K.);

Peppi.Karppinen@oulu.fi (P.K.)

Abstract (140 words)

Oxygen sensing is central to metazoan biology and has implications for human disease. Mammalian cells express multiple oxygen-dependent enzymes called 2-oxoglutarate (OG)-dependent dioxygenases (2-OGDDs), but they vary in their oxygen affinities and hence their ability to sense oxygen. The 2-OGDD histone demethylases control histone methylation. Hypoxia increases histone methylation, but whether this reflects direct effects on histone demethylases, or indirect effects caused by the hypoxic-induction of the HIF (Hypoxia-inducible Factor) transcription factor or the 2-OG antagonist 2-hydroxyglutarate (2-HG), is unclear. Here we report that hypoxia promotes histone methylation in a HIF- and 2-HG-independent manner. We found that the H3K27 histone demethylase KDM6A/UTX, but not its paralog KDM6B, is oxygen-sensitive. KDM6A loss, like hypoxia, prevented H3K27 demethylation and blocked cellular differentiation. Restoring H3K27 methylation homeostasis in hypoxic cells reversed these effects. Thus oxygen directly affects chromatin regulators to control cell fate.

Main Text (~2475 words)

Oxygen's appearance in earth's atmosphere was a watershed that created the evolutionary selection pressure for a conserved pathway used by metazoans to sense and respond to changes in ambient oxygen that converges on the heterodimeric HIF (Hypoxia-Inducible Factor) transcription factor. Under normoxic conditions, the HIFα subunit is prolyl hydroxylated by the EglN (Egg Laying-Defective Nine) isoenzymes of the 2-oxoglutarate (2-OG)-dependent dioxygenase family. Hydroxylated HIFα is earmarked for degradation by the von Hippel-Lindau (VHL) ubiquitin ligase complex. Hypoxia inactivates the EglNs and thereby stabilizes HIFα, which then associates with HIF1β [also called ARNT (Aryl Hydrocarbon Nuclear Translocator)] and transcriptionally activates genes that promote adaptation to inadequate oxygen (*1*).

The 2-OG-dependent dioxygenase family also includes the collagen prolyl hydroxylases, the JmjC (Jumonji C) domain histone Lysine Demethylases (KDMs), the Ten Eleven Translocation (TET) DNA hydroxylases, and ~50 other enzymes that are relatively understudied (*2*). In contrast to the high oxygen affinity (low K_M) collagen prolyl hydroxylases, the EglNs exhibit low oxygen affinities (high K_M) (*1*), which enables them to sense physiological changes in oxygen.

Several previous studies have suggested that oxygen regulates histone methylation. Certain KDMs display low oxygen affinities *in vitro (3)*. Moreover, many KDMs are transcriptionally activated by hypoxia and HIF (*4*), perhaps to compensate for a decrease in their enzymatic specific activity. Finally, hypoxia can induce histone hypermethylation (*5*). However, in these previous studies, it was unclear whether histone hypermethylation reflected a direct effect of hypoxia on KDMs or was confounded by indirect consequences of hypoxia (and HIF). For example, in some cells hypoxia increases the L-enantiomer of 2-hydroxyglutarate (L-2HG),

which is an endogenous inhibitor of 2-OG-dependent dioxygenases (*6-8*). Moreover, HIF can potentially affect chromatin in many ways, such as by altering KDM protein levels (*vide supra*), by inducing chromatin-modifying enzymes other than KDMs [e.g. TETs (*9*) and DNA methyltransferases (DNMTs) (*10*)], or by upregulating transcription factors that enforce an epithelial-mesenchymal transition (EMT) and accompanying epigenetic reprogramming (*11*).

To rigorously address whether hypoxia has a direct or indirect effect on histone methylation, we lentivirally transduced an *Arnt*-defective (HIF-inactive) mouse hepatoma cell line (mHepa-1 c4) to express either Green Fluorescent Protein (GFP), wild-type ARNT (WT), or a functionally inactive ARNT mutant (Δ414) that is missing 414 base pairs from its N-terminus, thereby eliminating its basic-Helix-Loop-Helix (bHLH) domain and ability to heterodimerize (Fig. 1A and fig. S1, A to C). mHepa-1 c4 did not tolerate prolonged growth in 1% oxygen, which is the oxygen concentration typically used to model hypoxia *ex vivo*. We therefore used more modest levels of hypoxia (2-5%) to study these cells. As expected, canonical HIF-target genes (e.g. *Egln3* and *Ndrg1*) were transcriptionally induced by 5% oxygen in the cells expressing wild-type ARNT, but not in the cells expressing ARNT (Δ 414) or GFP (fig. S1D).

We next used a multiplexed mass spectrometric assay (*12*) to quantify changes in histone methylation in response to hypoxia in the isogenic [GFP, ARNT(WT), ARNT(Δ 414)] mHepa-1 c4 cells. Unsupervised clustering of histone modification patterns revealed that the isogenic cell lines clustered primarily based on oxygen availability during growth and not HIF status (Fig. 1B). Consistent with prior reports (*5*), hypoxia promoted the dimethylation (me2) and trimethylation (me3) of H3K4 (histone 3, lysine 4), H3K9, and H3K27 (Fig. 1B). Hypermethylation of H3K9 and H3K27 was confirmed by immunoblot analysis (Fig. 1C). We also observed a concomitant decrease in hypomethylated H3K27 (me0/me1 states) and

acetylated H3K27, in response to hypoxia (Fig. 1B), which is consistent with the knowledge that histone methylation and acetylation are reciprocally regulated. The H3K27 hypermethylation was not explained by increased expression of EZH2 (enhancer of zeste homolog 2), which controls bulk H3K27 methylation, or decreased expression of the primary H3K27 histone demethylases KDM6A and KDM6B (fig. S2).

Hypoxia also promoted histone hypermethylation in *VHL*$^{-/-}$ RCC4 human renal carcinoma cells (fig. S3). Thus hypoxia promotes histone hypermethylation both in cells that cannot mount a HIF response (mHepa-1 c4 cells) and in cells that constitutively overproduce HIF (RCC4 cells), arguing that hypoxia's effects on histone methylation are not caused by changes in HIF activity.

We next explored whether hypoxia's effects on histone methylation in mHepa-1 c4 cells were caused by metabolic changes that can inhibit KDM activity, such as increased L-2HG or decreased 2-OG (*6-8, 13*). In the isogenic mHepa-1 c4 cells, 5% oxygen did not significantly induce either total 2-HG (fig. S4A), or enantiomer-specific 2-HG (fig. S4, B and C), and actually increased 2-OG levels (fig. S4D). 2-HG was modestly induced in parental mHepa-1 c4 cells by more profound levels of hypoxia (0.5-2% oxygen) (fig. S4, C and E), albeit as D-2HG rather than L-2HG (fig. S4C). The significance of the latter finding is unclear. Even under these more extreme conditions, the 2-HG levels achieved were ~100-fold below both the intracellular levels in mutant IDH1 (Isocitrate Dehydrogenase 1) cells (fig. S4F), wherein 2-HG serves as an oncometabolite (*14*), and the intracellular levels required to promote histone methylation in mHepa-1 c4 cells treated with cell-permeable versions of D-2HG or L-2HG (fig. S4, G and H). The latter observation is consistent with the biochemical D-2HG and L-2HG IC_{50} values for the KDMs (*15*).

Hypoxia can incite reactive oxygen species (ROS), which can inhibit 2-OG-dependent dioxygenases (*16*). Treating mHepa-1 c4 cells with the ROS-inducer *tert*-Butyl Hydroperoxide (tBHP) showed that intracellular ROS levels ~10-fold higher than those observed after exposure to 2% oxygen were required to induce histone methylation (fig. S5). These findings suggested that the HIF-independent effects of hypoxia on KDM activity were not caused by increased L-2HG, decreased 2-OG, or increased ROS, but instead were caused by a direct effect of hypoxia on the enzymatic activities of specific KDMs.

In support of this idea, we found that recombinant KDM4B, KDM5A, and KDM6A [also called Ubiquitously-Transcribed TPR Protein on the X chromosome (UTX)] have relatively low oxygen affinities that are comparable to the EglN family, whereas recombinant KDM4A, KDM5B, KDM5C, KDM5D, and KDM6B have high oxygen affinities (fig. S6 to S8). Finally, like full-length KDM6A, the isolated KDM6A catalytic domain also had low oxygen affinities compared to their KDM6B counterparts (Fig. 1, D to F, and fig. S8).

We focused our attention on the KDM6 H3K27 demethylases because hypoxia and histone H3K27 methylation have been independently linked to the control of cellular differentiation (*17-19*), because this histone mark can be manipulated with drugs, and because KDM6A has the lowest oxygen affinity of the KDMs tested to date. We first confirmed that hypoxia induced H3K27 methylation in additional human cell lines including 293T embryonic kidney cells, MCF7 breast cells, and SK-N-BE(2) neuroblastoma cells (fig. S9). Moreover, histological analysis showed elevated H3K27 methylation in mouse tissues that are known to be hypoxic, such as the kidney (*20*), splenic germinal centers (*21*), and thymus (*22*), but not in well-oxygenated tissues such as the heart (Fig. 1G). Similarly, H3K27 methylation is increased in hypoxic regions of mouse tumors (*23-25*) (fig. S10). Finally, Gene-Set Enrichment Analysis (*26*)

of ~2000 human tumors that were previously annotated as “Normoxic” or “Hypoxic” based on their HIF signature (*27*) (Table S1), revealed that “Hypoxic” tumors had transcriptional signatures indicative of H3K27 hypermethylation (fig. S11 and Tables, S2 and S3).

To examine the effect of hypoxia on cell differentiation *in vitro*, we studied C2C12 murine myoblasts. C2C12 differentiate into Myosin Heavy Chain (MyHC)-positive multinucleated myotubes when shifted from serum-rich growth media (GM) to nutrient-poor differentiation media (DM). Hypoxia blocks C2C12 differentiation (fig. S12, A to D) (*28, 29*). Hypoxic C2C12 cells grown in DM entered a quiescence-like state, but more readily proliferated when returned to GM under normoxic conditions compared to their normoxic counterparts (fig. S12, E to G). Similarly, hypoxia blocked the myogenic differentiation of mouse embryo fibroblasts (MEFs) that conditionally express MyoD (fig. S13).

Eliminating ARNT in C2C12 cells using CRISPR/Cas9 blocked (rather than accentuating) their ability to differentiate under normoxic conditions (fig. S14, A to C) and did not rescue their ability to differentiate under hypoxia (fig. S14D). Moreover, expression of stabilized versions of HIF1α or HIF2α did not block normoxic C2C12 differentiation (fig. S14, E and F). Thus, the differentiation block exhibited by hypoxia in C2C12 cells is not due to HIF activation.

Total 2-HG was not induced, and L-2HG was induced only about 2-fold (fig. S15, A to C), in C2C12 cells by 2% oxygen. C2C12 cells that were pharmacologically or genetically manipulated to have intracellular L-2HG levels 3-5-fold higher than observed under hypoxia still differentiated in DM (fig. S15, D to G). Therefore, hypoxia’s effects on C2C12 differentiation were not caused by 2-HG.

Similar to hypoxia, treatment of C2C12 cells with the KDM6 family inhibitor GSK-J4, promoted H3K27 hypermethylation and blocked myogenic differentiation (fig. S16). Similar results were obtained with MEFs expressing MyoD (fig. S13). In contrast, KDM-C70, a KDM5 family inhibitor, did not block C2C12 differentiation (fig. S17).

The differential oxygen affinities of KDM6A and KDM6B suggested that the ability of hypoxia to promote H3K27 methylation and block differentiation is caused specifically by a loss of KDM6A activity. Indeed, downregulating KDM6A, but not KDM6B, with different shRNAs, phenocopied the effects of hypoxia on differentiation (Fig. 2, A and B, and fig. S18, A to D) (*30*). Moreover, eliminating KDM6A in C2C12 cells with CRISPR/Cas9 blocked their ability to differentiate unless they were rescued with an sgRNA-resistant KDM6A cDNA (Fig. 2, C to E). In contrast, eliminating KDM6B had no effect (fig. S18, E and F) and eliminating KDM5A promoted differentiation (fig. S19). Notably, bulk H3K27me3 was oxygen-insensitive in the *Kdm6a*-deficient C2C12 cells, consistent with KDM6A being the primary oxygen sensor amongst the KDM6 paralogs (Fig. 2F).

Previous work showed that KDM6A is directly recruited to myogenic targets during differentiation (*30*). We therefore investigated whether differentiation programs driven by KDM6A activity involve transcriptional changes that depend on H3K27me3 elimination. Comparison of transcriptional signatures of normoxic C2C12 cells grown in GM *versus* DM revealed profound differences in transcriptional output, particularly of muscle-specific target genes (Fig. 2G, fig. S20, and Table S5). Hypoxia (and the consequent differentiation block), however, blunted the transcriptional differences between these two conditions (fig. S20A), which was associated with a failure of these cells to induce muscle-specific markers in DM (Fig. 2G and S20B). H3K27me3 status typically represses transcription. The inability of C2C12 cells

grown in DM to activate late myogenic genes (e.g. *Actc, Myl1*, and *Myog*) under hypoxia correlated with a failure to erase H3K27me3 at those loci (Fig 2, H to J and fig. S21), presumably due to inactivation of KDM6A. This was specific because H3K4me3 decreased at late myogenic genes under hypoxia (fig. S21).

Loss of cellular differentiation is a hallmark of cancer and *KDM6A* is a human tumor suppressor gene that is inactivated in a variety of cancers, including leukemia, kidney cancer, and bladder cancer (*31*). Remarkably, Gene Set Enrichment Analysis showed that a myogenic differentiation gene set, which presumably also contains genes linked to differentiation in other contexts, is more highly expressed in *KDM6*A wild-type bladder cancers compared to *KDM6A* mutant tumors (fig. S22 and Table S6).

These data suggest that KDM6A inactivation by hypoxia promotes the persistence of H3K27me3 and prevents the transcriptional reprogramming required for differentiation. If true, the effects of hypoxia on differentiation should be redressed by inhibiting H3K27 methyltransferase activity (Fig. 3A). Like mHepa-1 c4 cells, hypoxia did not alter the protein levels of the EZH H3K27 methyltransferases in C2C12 cells (fig. S23A). Inhibiting the H3K27 methyltransferase EZH2 with CRISPR/Cas9 (Fig. 3B and fig. S23B) or with the drug GSK126 (fig. S23, C and D) reduced H3K27me3 levels and partially rescued the ability of C2C12 cells to differentiate under hypoxic conditions. By contrast, the G9a/GLP methyltransferase inhibitor UNC638 was ineffective (fig. S23, C and D). Finally, GSK126 rescued the hypoxia-induced differentiation block in human primary myoblasts and in MEFs conditionally expressing MyoD (fig. S23, E and F).

Hypoxia can also, in a HIF-independent manner, alter the differentiation of human mammary epithelial (HMLE) cells (*25*), causing an EMT (fig. S24, A and B) and upregulation of

the cancer stem-like marker CD44 (fig. S24C). Similar to our findings with C2C12 cells, these hypoxia-associated changes were phenocopied by pharmacologic (GSK-J4) (fig. S24, A to C) or genetic (CRISPR/Cas9) disruption of KDM6A (fig. S24, D to F) and rescued by the EZH inhibitor GSK-126 (fig. S24, A to C).

Finally, we tried to directly increase KDM6A's oxygen affinity. We reasoned that certain non-conserved residues within the catalytic domains of KDM6A and KDM6B caused their vastly different oxygen affinities. We overlaid published models of the catalytic JmjC domains of KDM6A with KDM6B (*32, 33*) and noted two non-conserved residues, M^{1190} (KDM6A) → T^{1434} (KDM6B) and E^{1335} (KDM6A) → D^{1579} (KDM6B), lining the 2-OG- and Fe^{+2} binding-pocket (Fig. 3C). As predicted, a KDM6A variant that harbored these two "KDM6B-like" changes [MT/ED: M^{1190} → T and E^{1335}→ D], displayed a 2-fold increased affinity for oxygen *in vitro*, albeit at the cost of a decreased V_{max} (Fig. 3, D and E). Wild-type KDM6A and the MT/ED variant were comparably insensitive to L-2HG and to ROS (fig. S25, A to D), which was induced less than 2-fold by 2% oxygen in C2C12 cells (fig. S25E). Both wild-type KDM6A and the MT/ED rescued the ability of KDM6A-deficient C2C12 cells to differentiate under normoxia (fig. S26A). The double mutant, however, was superior to wild-type KDM6A at rescuing differentiation under hypoxic conditions in both parental and KDM6A-deficient C2C12 cells, presumably due to its enhanced oxygen affinity (Fig. 3, F and G, and fig. S26, B to D).

Independent lines of research have shown that oxygen and H3K27 methylation each regulate embryological development, cellular differentiation, stemness, and malignant transformation (*17-19*). We propose that these observations are linked. Specifically, we argue that oxygen has both direct and indirect effects on chromatin and that the former involves

enzymes such as KDM6A, which couple changes in oxygen availability to changes in H3K27 methylation and the transcriptional control of cell fate.

The observed H3K4 hypermethylation and H3K9 hypermethylation in hypoxic *Arnt*-deficient mHepa-1 c4 cells, together with our biochemical studies, suggests that at least one H3K4 and one H3K9 histone demethylase also act as oxygen sensors. For example, our biochemical data, together with the data in the accompanying manuscript (*34*), argue that KDM5A plays such a role. Profound hypoxia can also inhibit other 2-OG-dependent enzymes, including TETs, leading to DNA hypermethylation (*27*).

Mammalian embryological development occurs in a hypoxic environment and mammalian stem cells are maintained in hypoxic niches. It is well established that hypoxia can affect stemness and cellular differentiation by activating HIF and HIF-target genes such as *Oct4* (*19*). Such effects are not mutually exclusive with direct effects of oxygen on histone methylation and might serve to reinforce one another. Hypoxia promotes stemness in both metazoans and plants, but the HIF pathway is only present in the former (*35*). It is possible that oxygen sensing by histone demethylases evolutionarily preceded the emergence of oxygen-sensitive transcription factors.

List of Supplementary Materials:

Materials and Methods

Figures S1-S26

Tables S1-S6

References (*36-55*)

Figure Legends

Fig. 1. Hypoxia Causes HIF-Independent Histone Hypermethylation.

(**A**-**C**) Vector schematic (**A**), Histone modification profiling by mass spectrometry (**B**), and Histone immunoblot analysis (**C**) of *Arnt*-deficient mouse Hepatoma (mHepa-1 c4) cells that were lentivirally transduced to produce the indicated V5-tagged proteins and cultured at the indicated oxygen levels for 4 days. In (**B**), rows represent two biological replicates of the indicated samples and the color in each cell represents $\log_2$ fold change relative to all samples in the column, normalized for total histone using an internal control peptide (Histone H3: residues 41-49). (**D**-**F**) Coomassie blue staining (**D**) and biochemical analysis of baculovirally expressed and purified JumonjiC (JmjC) catalytic domains of KDM6A [KDM6A*] (**E**) and KDM6B [KDM6B*] (**F**). K_M values are mean +/- SD (N=3). (**G**) Immunohistochemical analysis of the indicated tissues derived from representative male and female age-matched mice

Fig. 2. Regulation of Myogenic Differentiation by the KDM6A H3K27 Demethylase.

(**A**-**B**) Immunofluorescence analysis of C2C12 cells that were lentivirally transduced to express the shRNAs targeting *Kdm6A* (**A**) or *Kdm6B* (**B**) and then cultured in differentiation media for 4 days. (**C**-**E**) Immunoblot analysis of C2C12 cells lentivirally transduced to express the indicated sgRNAs and cultured for 4 days either in growth media (GM) or differentiation media (DM), as indicated. (**E**) Immunoblot analysis of C2C12 cells expressing, where indicated, *Kdm6a* sg2 [described in (**C**) and (**D**)] that were lentivirally transduced to produce either GFP (control) or wild-type human KDM6A [6A(WT)] and then cultured in DM at the indicated oxygen concentrations for 4 days. The mouse *Kdm6A* sg2 target sequence is not conserved in human *KDM6A*. (**F**) Immunoblot analysis of histones from C2C12 cells expressing the indicated sgRNA that were cultured at the indicated oxygen concentrations for 3 days. (**G**-**J**) Heatmap representing

mRNA levels determined by RNA-Seq (**G**) and H3K27me3 levels determined by ChIP-Seq analysis at the *Actc1* (**H**), *Myl1* (**I**), and the *Myog* (**J**) loci from two biological replicates (A and B) of C2C12 cells cultured in the indicated media for 4 days at the indicated oxygen concentration.

Fig. 3. Restoring the Balance of H3K27 Methyltransferase Activity to H3K27 Demethylase Activity Rescues Myogenic Differentiation Under Hypoxic Conditions.

(**A**) Model for control of H3K27 methylation by the indicated opposing demethylases ("erasers") and methyltransferases ("writers"). (**B**) Immunoblot analysis of C2C12 cells lentivirally transduced to express the indicated sgRNAs and cultured under the indicated conditions. (**C**) Structural models of the KDM6A (pink) and KDM6B (cyan) catalytic pockets. The non-conserved M^{1190} (KDM6A) → T^{1434} (KDM6B) and the E^{1335} (KDM6A) → D^{1579} (KDM6B) are highlighted. Peptidic H3K27me3 substrate (yellow), Fe^{+2} (orange), 2-oxoglutarate (green), and Zn^{+2} (grey) are shown. (**D**-**E**) Michaelis-Menten plots (inset Lineweaver-Burk plot) and measured oxygen K_M and V_{max} values (mean +/- SD, N=3) of recombinant KDM6A wild-type and the MT/ED mutant. (**F**-**G**) Real-Time qPCR analysis (mean +/- SD, N =3) of the indicated genes (**F**) and immunofluorescence analysis (**G**) of C2C12 cells transduced to produce wild-type human KDM6A or the KDM6A MT/ED variant and then cultured in DM at the indicated oxygen concentrations for 4 days.

References and Notes

1. W. G. Kaelin, Jr., The von Hippel-Lindau tumour suppressor protein: O2 sensing and cancer. *Nature reviews. Cancer* **8**, 865 (2008).
2. M. A. McDonough, C. Loenarz, R. Chowdhury, I. J. Clifton, C. J. Schofield, Structural studies on human 2-oxoglutarate dependent oxygenases. *Current opinion in structural biology* **20**, 659 (2010).
3. R. L. Hancock, K. Dunne, L. J. Walport, E. Flashman, A. Kawamura, Epigenetic regulation by histone demethylases in hypoxia. *Epigenomics* **7**, 791 (2015).
4. A. Melvin, S. Rocha, Chromatin as an oxygen sensor and active player in the hypoxia response. *Cellular signalling* **24**, 35 (2012).
5. A. Shmakova, M. Batie, J. Druker, S. Rocha, Chromatin and oxygen sensing in the context of JmjC histone demethylases. *The Biochemical journal* **462**, 385 (2014).
6. A. M. Intlekofer *et al.*, Hypoxia Induces Production of L-2-Hydroxyglutarate. *Cell metabolism* **22**, 304 (2015).
7. W. M. Oldham, C. B. Clish, Y. Yang, J. Loscalzo, Hypoxia-Mediated Increases in L-2-hydroxyglutarate Coordinate the Metabolic Response to Reductive Stress. *Cell metabolism* **22**, 291 (2015).
8. P. A. Tyrakis *et al.*, S-2-hydroxyglutarate regulates CD8+ T-lymphocyte fate. *Nature* **540**, 236 (2016).
9. C. J. Mariani *et al.*, TET1-mediated hydroxymethylation facilitates hypoxic gene induction in neuroblastoma. *Cell reports* **7**, 1343 (2014).
10. C. J. Watson *et al.*, Hypoxia-induced epigenetic modifications are associated with cardiac tissue fibrosis and the development of a myofibroblast-like phenotype. *Human molecular genetics* **23**, 2176 (2014).
11. D. F. Higgins *et al.*, Hypoxia promotes fibrogenesis in vivo via HIF-1 stimulation of epithelial-to-mesenchymal transition. *The Journal of clinical investigation* **117**, 3810 (2007).
12. A. L. Creech *et al.*, Building the Connectivity Map of epigenetics: chromatin profiling by quantitative targeted mass spectrometry. *Methods* **72**, 57 (2015).
13. B. W. Carey, L. W. Finley, J. R. Cross, C. D. Allis, C. B. Thompson, Intracellular alpha-ketoglutarate maintains the pluripotency of embryonic stem cells. *Nature* **518**, 413 (2015).
14. J. A. Losman, W. G. Kaelin, Jr., What a difference a hydroxyl makes: mutant IDH, (R)-2-hydroxyglutarate, and cancer. *Genes & development* **27**, 836 (2013).
15. T. Laukka, M. Myllykoski, R. E. Looper, P. Koivunen, Cancer-associated 2-oxoglutarate analogues modify histone methylation by inhibiting histone lysine demethylases. *Journal of molecular biology* **430**, 3081 (2018).
16. W. G. Kaelin, Jr., ROS: really involved in oxygen sensing. *Cell metabolism* **1**, 357 (2005).
17. E. Conway, E. Healy, A. P. Bracken, PRC2 mediated H3K27 methylations in cellular identity and cancer. *Current opinion in cell biology* **37**, 42 (2015).
18. S. Manna *et al.*, Histone H3 Lysine 27 demethylases Jmjd3 and Utx are required for T-cell differentiation. *Nature communications* **6**, 8152 (2015).
19. A. Mohyeldin, T. Garzon-Muvdi, A. Quinones-Hinojosa, Oxygen in stem cell biology: a critical component of the stem cell niche. *Cell stem cell* **7**, 150 (2010).

20. M. Safran *et al.*, Mouse model for noninvasive imaging of HIF prolyl hydroxylase activity: assessment of an oral agent that stimulates erythropoietin production. *Proceedings of the National Academy of Sciences of the United States of America* **103**, 105 (2006).
21. S. H. Cho *et al.*, Germinal centre hypoxia and regulation of antibody qualities by a hypoxia response system. *Nature* **537**, 234 (2016).
22. L. P. Hale, R. D. Braun, W. M. Gwinn, P. K. Greer, M. W. Dewhirst, Hypoxia in the thymus: role of oxygen tension in thymocyte survival. *American journal of physiology. Heart and circulatory physiology* **282**, H1467 (2002).
23. M. E. Adriaens *et al.*, Quantitative analysis of ChIP-seq data uncovers dynamic and sustained H3K4me3 and H3K27me3 modulation in cancer cells under hypoxia. *Epigenetics & chromatin* **9**, 48 (2016).
24. P. Prickaerts *et al.*, Hypoxia increases genome-wide bivalent epigenetic marking by specific gain of H3K27me3. *Epigenetics & chromatin* **9**, 46 (2016).
25. T. van den Beucken *et al.*, Hypoxia promotes stem cell phenotypes and poor prognosis through epigenetic regulation of DICER. *Nature communications* **5**, 5203 (2014).
26. A. Subramanian *et al.*, Gene set enrichment analysis: a knowledge-based approach for interpreting genome-wide expression profiles. *Proceedings of the National Academy of Sciences of the United States of America* **102**, 15545 (2005).
27. B. Thienpont *et al.*, Tumour hypoxia causes DNA hypermethylation by reducing TET activity. *Nature* **537**, 63 (2016).
28. A. J. Majmundar *et al.*, O(2) regulates skeletal muscle progenitor differentiation through phosphatidylinositol 3-kinase/AKT signaling. *Molecular and cellular biology* **32**, 36 (2012).
29. Z. Yun, Q. Lin, A. J. Giaccia, Adaptive myogenesis under hypoxia. *Molecular and cellular biology* **25**, 3040 (2005).
30. S. Seenundun *et al.*, UTX mediates demethylation of H3K27me3 at muscle-specific genes during myogenesis. *The EMBO journal* **29**, 1401 (2010).
31. L. D. Ler *et al.*, Loss of tumor suppressor KDM6A amplifies PRC2-regulated transcriptional repression in bladder cancer and can be targeted through inhibition of EZH2. *Science translational medicine* **9**, (2017).
32. L. Kruidenier *et al.*, A selective jumonji H3K27 demethylase inhibitor modulates the proinflammatory macrophage response. *Nature* **488**, 404 (2012).
33. T. Sengoku, S. Yokoyama, Structural basis for histone H3 Lys 27 demethylation by UTX/KDM6A. *Genes & development* **25**, 2266 (2011).
34. M. Batie *et al.*, Hypoxia induces rapid changes to histone methylation reprogramming chromatin for the cellular response, *Science* xxx, xx (2019)
35. M. J. Considine *et al.*, Learning To Breathe: Developmental Phase Transitions in Oxygen Status. *Trends in plant science* **22**, 140 (2017).
36. D. Rohle *et al.*, An inhibitor of mutant IDH1 delays growth and promotes differentiation of glioma cells. *Science* **340**, 626 (2013).
37. P. Koivunen *et al.*, Transformation by the (R)-enantiomer of 2-hydroxyglutarate linked to EGLN activation. *Nature* **483**, 484 (2012).
38. H. Wakimoto *et al.*, Targetable signaling pathway mutations are associated with malignant phenotype in IDH-mutant gliomas. *Clinical cancer research : an official journal of the American Association for Cancer Research* **20**, 2898 (2014).

39. R. Varaljai *et al.*, Increased mitochondrial function downstream from KDM5A histone demethylase rescues differentiation in pRB-deficient cells. *Genes & development* **29**, 1817 (2015).
40. A. M. Intlekofer *et al.*, L-2-Hydroxyglutarate production arises from noncanonical enzyme function at acidic pH. *Nature chemical biology* **13**, 494 (2017).
41. M. Hirsila, P. Koivunen, V. Gunzler, K. I. Kivirikko, J. Myllyharju, Characterization of the human prolyl 4-hydroxylases that modify the hypoxia-inducible factor. *The Journal of biological chemistry* **278**, 30772 (2003).
42. K. I. Kivirikko, R. Myllyla, Posttranslational enzymes in the biosynthesis of collagen: intracellular enzymes. *Methods in enzymology* **82 Pt A**, 245 (1982).
43. A. Dobin *et al.*, STAR: ultrafast universal RNA-seq aligner. *Bioinformatics* **29**, 15 (2013).
44. C. Trapnell *et al.*, Transcript assembly and quantification by RNA-Seq reveals unannotated transcripts and isoform switching during cell differentiation. *Nature biotechnology* **28**, 511 (2010).
45. M. Cornwell *et al.*, VIPER: Visualization Pipeline for RNA-seq, a Snakemake workflow for efficient and complete RNA-seq analysis. *BMC bioinformatics* **19**, 135 (2018).
46. Q. Qin *et al.*, ChiLin: a comprehensive ChIP-seq and DNase-seq quality control and analysis pipeline. *BMC bioinformatics* **17**, 404 (2016).
47. J. T. Robinson *et al.*, Integrative genomics viewer. *Nature biotechnology* **29**, 24 (2011).
48. B. Langmead, S. L. Salzberg, Fast gapped-read alignment with Bowtie 2. *Nature methods* **9**, 357 (2012).
49. P. V. Kharchenko, M. Y. Tolstorukov, P. J. Park, Design and analysis of ChIP-seq experiments for DNA-binding proteins. *Nature biotechnology* **26**, 1351 (2008).
50. J. Casper *et al.*, The UCSC Genome Browser database: 2018 update. *Nucleic acids research* **46**, D762 (2018).
51. H. Mi *et al.*, PANTHER version 11: expanded annotation data from Gene Ontology and Reactome pathways, and data analysis tool enhancements. *Nucleic acids research* **45**, D183 (2017).
52. C. The Gene Ontology, Expansion of the Gene Ontology knowledgebase and resources. *Nucleic acids research* **45**, D331 (2017).
53. M. Deng, J. Bragelmann, I. Kryukov, N. Saraiva-Agostinho, S. Perner, FirebrowseR: an R client to the Broad Institute's Firehose Pipeline. *Database : the journal of biological databases and curation* **2017**, (2017).
54. K. Numayama-Tsuruta, A. Kobayashi, K. Sogawa, Y. Fujii-Kuriyama, A point mutation responsible for defective function of the aryl-hydrocarbon-receptor nuclear translocator in mutant Hepa-1c1c7 cells. *European journal of biochemistry* **246**, 486 (1997).
55. W. Y. Kim *et al.*, Failure to prolyl hydroxylate hypoxia-inducible factor alpha phenocopies VHL inactivation in vivo. *The EMBO journal* **25**, 4650 (2006).

ACKNOWLEDGMENTS

We thank H. Zhao, D. Lambrechts, and P. Carmeliet for sharing their TCGA tumor annotations. We thank R. Looper for synthesizing and sharing the esterified 2-HG. M. K. Koski and R. Wierenga for help with structural modeling, and T. Aatsinki and E. Lehtimaki for technical assistance. We thank the Broad GDAC group for help with the GDAC-GSEA source code. We thank M. Oser for sharing mouse KDM5A sgRNAs and V. Koduri for assistance in acquiring microscopic images. **Funding:** WGK was supported by grants from the NIH (R01CA068490, P50CA101942, and R35CA210068). AAC was supported by grants from the 'Friends of Dana-Farber' and the NIH (Cancer Biology Training grant: T32CA009361 and the DF/HCC Kidney SPORE CEP and DRP award: P50CA101942). PK was supported by Academy of Finland Grants 266719 and 308009, the S. Juselius Foundation, the Jane and Aatos Erkko Foundation, and the Finnish Cancer Organizations. TL was supported by the Finnish Medical Foundation and, with PK, the Emil Aaltonen Foundation. S.K.M. is supported by an American Cancer Society postdoctoral fellowship (PF-14-144-01-TBE) and by a Career Enhancement Project award from the Dana-Farber/Harvard Cancer Center Brain SPORE. WGK is a HHMI Investigator. **Author Contributions:** A.A.C.. P.K., and W.G.K. conceived experiments and wrote the manuscript, A.A.C, T.L., M.M., A.E.R., A.C., R.J., and J.S. performed experiments. A.A.C., T.L., M.M, A.E.R, M.A.B, M.Y.T, Y.J.M., S.M., S.K.M, B.O., Z.T.H, S.M., J.J., S.S., M.H., R.B., P.K., and W.G.K. analyzed data. **Competing Interests:** W.G.K. has financial interests related to Lilly Pharmaceuticals (Board of Directors), Agio Pharmaceuticals [Scientific Advisory Board (SAB)], Cedilla Therapeutics (Founder), Fibrogen (SAB), Nextech Invest (SAB), Peloton Therapeutics (SAB), Tango Therapeutics (Founder), and Tracon Pharmaceuticals (SAB). W.G.K. is a coinventor on a patent entitled "Pharmaceuticals and Methods for Treating Hypoxia and

Screening Methods Therefor" that has been licensed to Fibrogen. S. S. has a consulting or advisory role in AstraZeneca/MedImmune, Merck, AACR, and NCI; patents, royalties, other intellectual property from Biogenex Laboratories; and research funding from AstraZeneca, Exelixis, Bristol-Myers Squibb. R.B receives research funding from Novartis. **Data and materials availability:** All data are available in the manuscript or the supplementary material. RNA-Seq and ChIP-Seq data have been uploaded to the GEO (GSE114086).

FIGURE 1

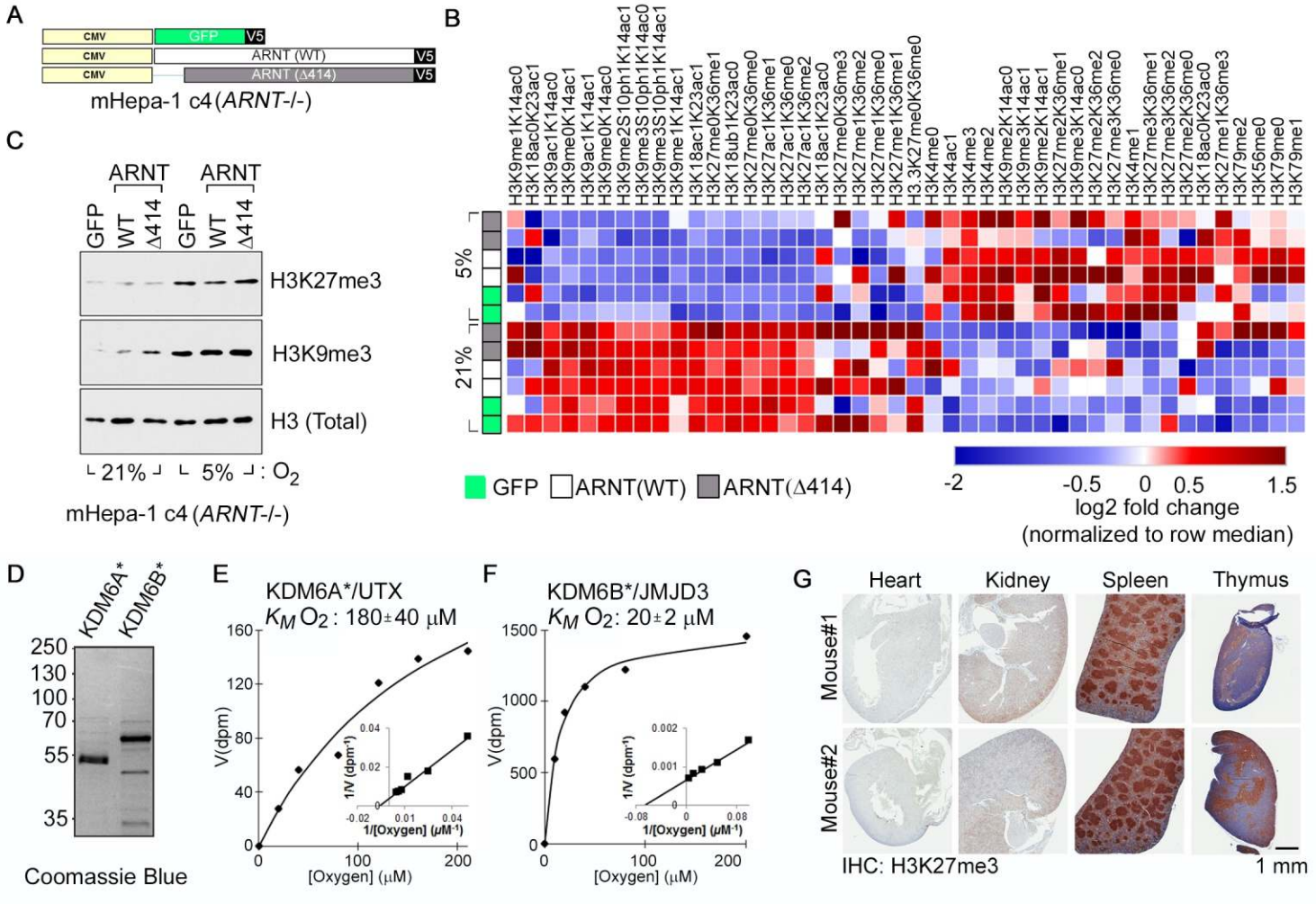
A
CMV
GFP
V5
ARNT (WT)
ARNT (Δ414)
mHepa-1 c4 (ARNT-/-)
B
H3K9me1K14ac0
H3K18ac0K23ac1
H3K9ac1K14ac0
H3K9me0K14ac1
H3K9ac1K14ac1
H3K9me0K14ac0
H3K9me2S10ph1K14ac1
H3K9me3S10ph1K14ac0
H3K9me3S10ph1K14ac1
H3K9me1K14ac1
H3K18ac1K23ac1
H3K27me0K36me1
H3K18ub1K23ac0
H3K27me0K36me0
H3K27ac1K36me1
H3K27ac1K36me0
H3K27ac1K36me2
H3K18ac1K23ac0
H3K27me0K36me3
H3K27me1K36me2
H3K27me1K36me0
H3K27me1K36me1
H3.3K27me0K36me0
H3K4me0
H3K4ac1
H3K4me3
H3K4me2
H3K9me2K14ac0
H3K9me3K14ac1
H3K9me2K14ac1
H3K27me2K36me1
H3K9me3K14ac0
H3K27me2K36me2
H3K27me3K36me0
H3K4me1
H3K27me3K36me1
H3K27me3K36me2
H3K27me2K36me0
H3K18ac0K23ac0
H3K27me1K36me3
H3K79me2
H3K56me0
H3K79me0
H3K79me1
5%
21%
GFP
ARNT(WT)
ARNT(Δ414)
-2
-0.5
0
0.5
1.5
log2 fold change
(normalized to row median)
C
ARNT
ARNT
GFP
WT
Δ414
GFP
WT
Δ414
H3K27me3
H3K9me3
H3 (Total)
21%
5%
: O2
mHepa-1 c4 (ARNT-/-)
D
KDM6A*
KDM6B*
250
130
100
70
55
35
Coomassie Blue
E
KDM6A*/UTX
KM O2 : 180±40 μM
V(dpm)
[Oxygen] (μM)
1/V (dpm-1)
1/[Oxygen] (μM-1)
F
KDM6B*/JMJD3
KM O2: 20±2 μM
V(dpm)
[Oxygen] (μM)
1/V (dpm-1)
1/[Oxygen] (μM-1)
G
Heart
Kidney
Spleen
Thymus
Mouse#1
Mouse#2
IHC: H3K27me3
1 mm

FIGURE 2

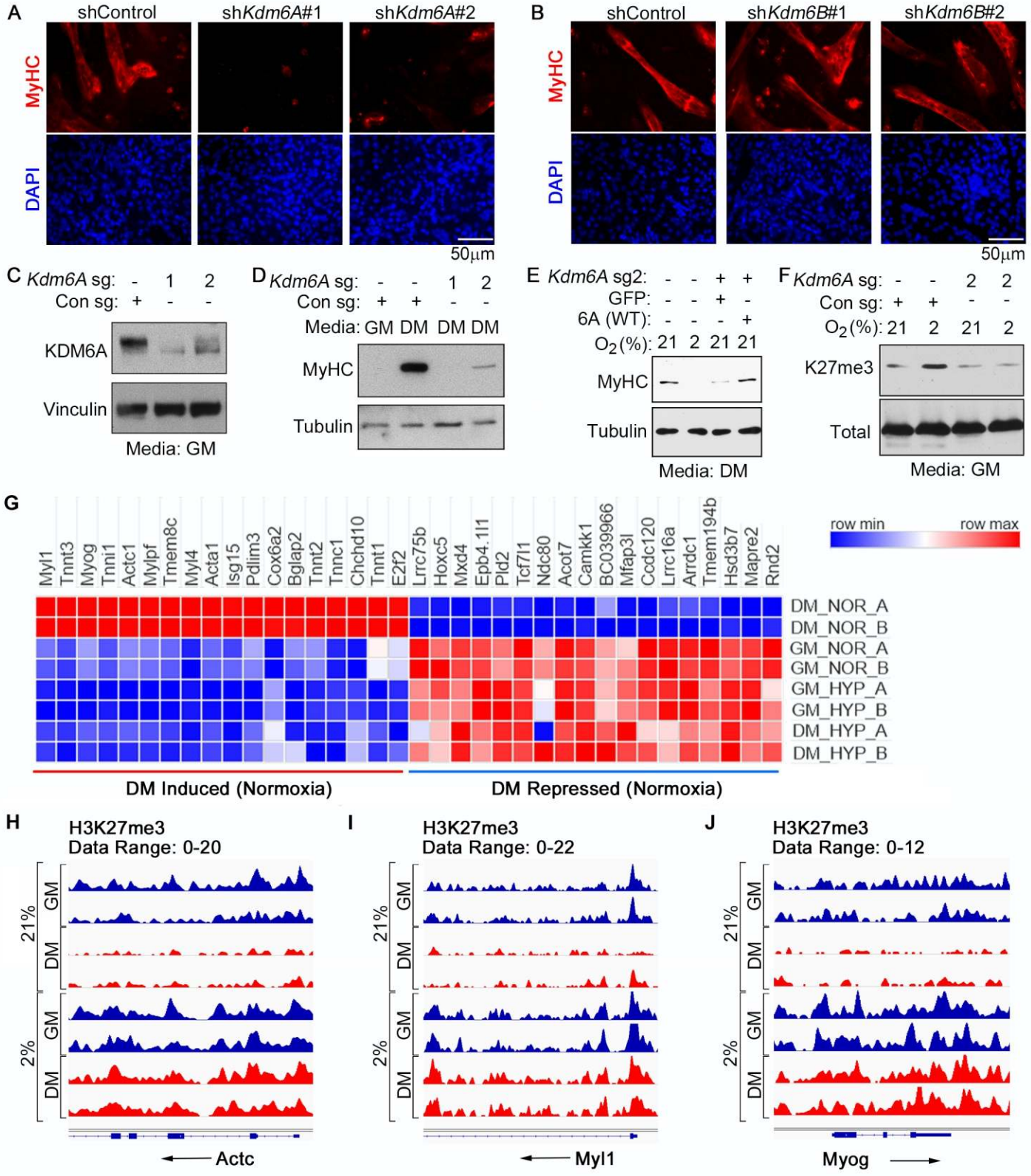
A
shControl
shKdm6A#1
shKdm6A#2
MyHC
DAPI
50μm
B
shControl
shKdm6B#1
shKdm6B#2
MyHC
DAPI
50μm
C
Kdm6A sg: - 1 2
Con sg: + - -
KDM6A
Vinculin
Media: GM
D
Kdm6A sg: - - 1 2
Con sg: + + - -
Media: GM DM DM DM
MyHC
Tubulin
E
Kdm6A sg2: - - + +
GFP: - - + -
6A (WT): - - - +
O2(%): 21 2 21 21
MyHC
Tubulin
Media: DM
F
Kdm6A sg: - - 2 2
Con sg: + + - -
O2(%): 21 2 21 2
K27me3
Total
Media: GM
G
Myl1 Tnnt3 Myog Tnni1 Actc1 Mylpf Tmem8c Myl4 Acta1 Isg15 Pdlim3 Cox6a2 Bglap2 Tnnt2 Tnnc1 Chchd10 Tnnt1 E2f2
Lrrc75b Hoxc5 Mxd4 Epb4.1l1 Pld2 Tcf7l1 Ndc80 Acot7 Camkk1 BC039966 Mfap3l Ccdc120 Lrrc16a Arrdc1 Tmem194b Hsd3b7 Mapre2 Rnd2
row min
row max
DM_NOR_A
DM_NOR_B
GM_NOR_A
GM_NOR_B
GM_HYP_A
GM_HYP_B
DM_HYP_A
DM_HYP_B
DM Induced (Normoxia)
DM Repressed (Normoxia)
H
H3K27me3
Data Range: 0-20
21%
2%
GM
DM
Actc
I
H3K27me3
Data Range: 0-22
Myl1
J
H3K27me3
Data Range: 0-12
Myog

FIGURE 3

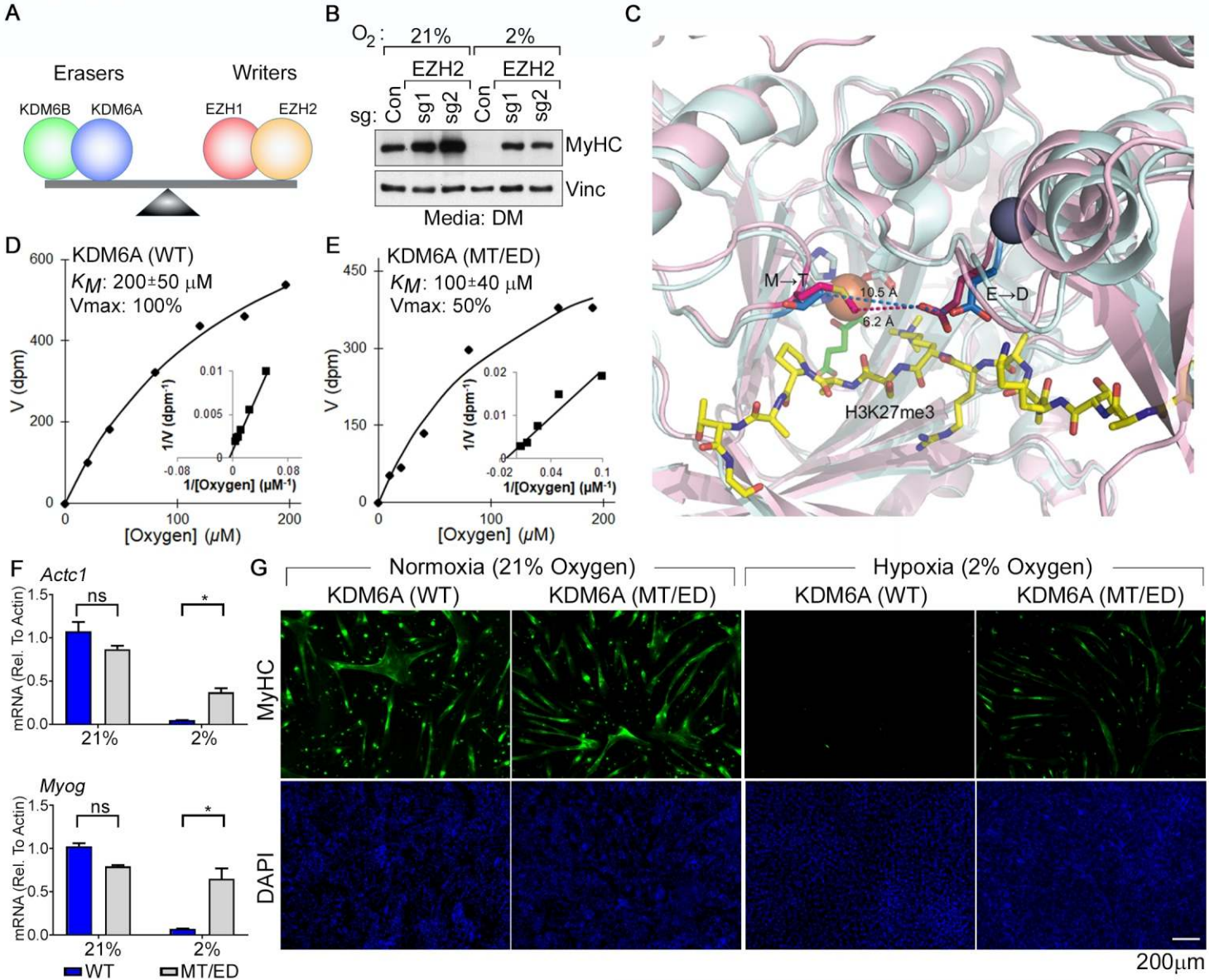
A
Erasers
Writers
KDM6B
KDM6A
EZH1
EZH2
B
O2: 21% 2%
EZH2 EZH2
sg: Con sg1 sg2 Con sg1 sg2
MyHC
Vinc
Media: DM
C
M→T
E→D
10.5 Å
6.2 Å
H3K27me3
D
KDM6A (WT)
KM: 200±50 μM
Vmax: 100%
V (dpm)
[Oxygen] (μM)
1/V (dpm-1)
1/[Oxygen] (μM-1)
E
KDM6A (MT/ED)
KM: 100±40 μM
Vmax: 50%
V (dpm)
[Oxygen] (μM)
1/V (dpm-1)
1/[Oxygen] (μM-1)
F
Actc1
mRNA (Rel. To Actin)
ns
*
21%
2%
Myog
mRNA (Rel. To Actin)
ns
*
21%
2%
WT
MT/ED
G
Normoxia (21% Oxygen)
Hypoxia (2% Oxygen)
KDM6A (WT)
KDM6A (MT/ED)
KDM6A (WT)
KDM6A (MT/ED)
MyHC
DAPI
200μm

Science
AAAS

Supplementary Materials for

Title: Histone demethylase KDM6A directly senses oxygen to control chromatin and cell fate

Authors: Abhishek A. Chakraborty, Tuomas Laukka, Matti Myllykoski, Alison E. Ringel, Matthew A. Booker, Michael Y. Tolstorukov, Yuzhong Jeff Meng, Samuel R. Meier, Rebecca B. Jennings, Amanda L. Creech, Zachary T. Herbert, Jessica Spinelli, Samuel K. McBrayer, Benjamin A. Olenchock, Jacob D. Jaffe, Marcia C. Haigis, Rameen Beroukhim, Sabina Signoretti, Peppi Koivunen, and William G. Kaelin, Jr.

Correspondence to:

W.G.K (william_kaelin@dfci.harvard.edu) or P.K. (Peppi.Karppinen@oulu.fi)

This PDF file includes:

Materials and Methods

Figs. S1 to S26

Other Supplementary Materials for this manuscript include the following:

Tables S1 to S6

MATERIALS AND METHODS

Cell lines

The C2C12 cells (CRL-1772), MCF7 cells (HTB-22), and 293T cells (CRL-3216) were obtained from ATCC. The mHepa-1 c4 cells (a gift of Dr. Oliver Hankinson) were maintained in Minimum Essential Medium (MEM) alpha with Earle's salts supplemented with 10% fetal bovine serum (FBS) (Life Technologies 10437-028) and 1X penicillin-streptomycin (Life Technologies 15140163). C2C12 and RCC4 cells (a gift of Dr. Peter Ratcliffe) were maintained in Dulbecco's Modified Eagle's Medium (DMEM) (Life Technologies) supplemented with 10% FBS and 1X penicillin-streptomycin. The 293T cells were maintained in Dulbecco's Modified Eagle's Medium (DMEM) (Merck) supplemented with 10% FBS, 2 mM L-glutamine (Sigma G7513), 0.375 % Na-bicarbonate (Biowest L0680), and 1X penicillin-streptomycin (Sigma P0781). The 293T media supplemented with 10 µg/ml insulin was used to culture MCF7 cells. The SK-N-BE(2) cells, a gift ftom Dr. Lucy Godley at University of Chicago, were maintained in RPMI1640 media (ThermoFisher). The glioma cell lines TS603 and TS516 (a gift of Dr. Ingo Mellinghoff at MSKCC) (*36*) and the BT260 cells (a gift of Dr. Keith Ligon at DFCI) (*37*), were cultured in NeuroCult NS-A Basal Medium with Proliferation Supplement (StemCell Technologies) supplemented with EGF (20 ng/ml), bFGF (20 ng/ml), heparin (2 µg/ml), 1% penicillin/streptomycin, Fungizone (250 ng/ml), and Plasmocin (2.5 µg/ml). The glioma cell line MGG152 (a gift of Dr. Daniel Cahill at MGH) (*38*), was cultured in Neurobasal Medium supplemented with 3 mM glutamine, 1X B27, 0.25X N2, EGF (20 ng/ml), bFGF (20 ng/ml), heparin (2 µg/ml), 1% penicillin/streptomycin, and Fungizone (250 ng/ml). All glioma cell lines were passaged as neurospheres and dissociated 1-2 times per week. The Mouse Embryonic Fibroblasts expressing MyoD-ER, a kind gift from Dr. Benevolenskaya (U. of Illinois, Chicago)

(*39*), were cultured in DMEM supplemented with 10% Calf Serum and 1X Penicillin/Streptomycin. The primary Human Skeletal Myoblasts (HSkM) were purchased from Gibco (A12555) and cultured in Complete Skeletal Muscle Media (ZenBio). The human mammary epithetelial cells (HMLE) were a kind gift from Dr. William Hahn and were cultured in MEBM basal Medium (Lonza CC-3151) supplemented with growth factors (MEGM Singlequot, Lonza CC-4136). Lentivirally infected cells were selected with puromycin (2 µg/ml) or blasticidin (10 µg/ml) as appropriate for the vector used. All mammalian cells were grown at 37°C in 5% CO_2. The *Sf9* insect cells were cultured in TNM-FH media supplemented with 10% FBS and cultured at 27°C.

Plasmids

The pLX304-GFP (ccsbBroad304_99986) vector was obtained from the Gene Pertubation Platform (GPP, Broad Institute). The pLX304 ARNT expression plasmids were made by sub-cloning the human ARNT cDNA (wild-type or with a 5' 414 bp deletion [Δ414]) generated by PCR amplification into the pLX304 destination vector (Addgene # 25890) using Gateway cloning. The pLKO-based plasmids to express shRNAs targeting *Kdm6a* (#1: TRCN0000107762 and #2: TRCN0000107762) and *Kdm6b* (#1: TRCN0000236677 and #2: TRCN0000236678) were obtained from the GPP, Broad Institute. The pLenti-EF1α-Vec, pLenti-HIF1αdPA, and pLenti-HIF2αdPA plasmids were a gift from Dr. Julie Losman at Dana-Farber Cancer Institute.

The baculovirus for C-terminal FLAG-tagged human KDM5B was a gift from Dr. Qin Yan at Yale University. Human full length KDM4A and KDM4B in the pReceiver-I01 plasmid, a gift from Dr. Susanne Schlisio at Karolinska Institute, were used to generate the corresponding

baculoviruses with N-terminal His-tags. FLAG-tagged human full length KDM5A, KDM6A, KDM6B, and the JumonjiC-domains of KDM6A (931→End) and KDM6B (1164→End) were generated by PCR and subcloned into the pVL1393 backbone. The KDM6A M→T/E→D mutant was generated via site-directed mutagenesis of pVL1393-KDM6A-FLAG using the QuickChange® Lightning site-directed mutagenesis kit (Stratagene) according to the manufacturer's protocol and confirmed by Sanger DNA sequencing. The corresponding baculoviruses with C-terminal FLAG-tags were generated using the BacMagic-3 DNA kit (Novagen). The FLAG-tagged full-length human KDM5C and KDM5D were generated by PCR and subcloned into pFastBac Dual plasmid. KDM5C and KDM5D bacmids were generated using DH10Bac cells with the standard Bac-to-Bac protocol (Invitrogen) and the corresponding baculoviruses were generated by transfecting the bacmid DNA into Sf9 cells.

The pLX304-WT KDM6A expression vector was made by subcloning a human KDM6A cDNA generated by PCR amplification of pCMV-HA-UTX (Addgene#24168) into the pLX304 destination vector by Gateway cloning. pLX304 expression plasmids encoding UTX/KDM6A mutants were made by site-directed mutagenesis (Quickchange II XL; Agilent 200521) of pLX304-KDM6A according to the manufacturer's recommendations and confirmed by Sanger DNA sequencing. The pLenti-CRISPRv2 (Addgene # 52961) sgRNA expression plasmids were made by cloning annealed duplex oligonucleotides (see table S1) into BsmBI-digested pLenti-CRISPRv2. All primer sequences used for cloning, mutagenesis, and Real-Time qPCR analysis are provided in the table below.

Histone extraction for immunoblotting and mass spectrometry profiling

To prepare crude histone extracts for immunoblotting, soluble subcellular fractions were eliminated by lysing cells twice in nucleus buffer (15 mM Tris [pH 7.5], 250 mM Sucrose, 60 mM KCl, 15 mM NaCl, 5 mM $MgCl_2$, and 1 mM $CaCl_2$) supplemented with 0.5% NP-40, 1 mM DTT, 10 mM sodium butyrate, and protease inhibitor cocktail (Roche, 29384100). Soluble fractions were discarded by centrifugation at 8000 rcf for 5 min at 4°C. The insoluble (chromatin-enriched) fractions were acid extracted with 0.2N HCl for >6 hours (typically overnight) at 4°C. For immunoblot analysis the histone preparations were quantified using the Protein Assay Dye Reagent (Biorad 500-0006) and 200 ng histone from each sample was analyzed per lane.

Global Chromatin Profiling (GCP) assay (*12*) was used to measure bulk differences in histone modifications. This assay simultaneously quantifies many histone modifications by comparing their abundance on tryptic digests of Histone H3 to spiked-in internal control peptides harboring the corresponding modification. For these assays, crude histone preparations (generated as described above) were further purified by TCA precipitation. The precipitated histones were derivatized with NHS-propionate, digested by trypsinization, rederivatized, and modification profiles were generated by mass spectrometric comparison to a spiked-in internal standard peptide for the modification of interest as previously described (*12*).

Immunoblot and Immunoprecipitation analysis

Cells were lysed in lysis buffer (50 mM Tris HCl [pH 7.5], 400 mM NaCl, 1% Nonidet P-40, 1 mM EDTA, and 10% glycerol) supplemented with a protease inhibitor cocktail (PIC, Complete mini EDTA-Free, Roche) and a phosphatase inhibitor cocktail (PhosSTOP, Roche).

For immunoprecipitation analysis, 750 µg of total protein was diluted to a total volume of 1 ml, of which 10% (100 µl) was kept aside as "Input", and the remainder was tumbled in the presence of 30 µl 50% anti-V5 sepharose (Sigma A7345) for 3 hours at 4°C. Bound beads were washed 4 times in lysis buffer, boiled in 100 µl of 1X SDS buffer (0.0005% Bromophenol Blue in 50 mM Tris HCl [pH 6.8], 0.15% β-Mercaptoethanol, 2% SDS, and 10% Glycerol), and resolved by SDS-PAGE. For immunoblot analysis, lysates prepared in 1X SDS buffer were resolved using 6%, 8%, or 15% SDS-PAGE gels, as appropriate, and transferred onto 0.2 µM nitrocellulose membranes.

The following primary antibodies were used for immunoblot analysis: Actin (Cell Signaling 4970, 1:5000), ARNT (Cell Signaling 5537, 1:1000), Cyclin E (Cell Signaling 4129, 1:1000), EZH1 (Novus 56358), EZH2 (Cell Signaling 5246, 1:1000), HIF1α (Cell Signaling 14179, 1:1000), Histone H3K27me3 (Cell Signaling 9733, 1:2000), Histone H3K4me3 (Cell Signaling 9727, 1:2000), Histone H3K9me3 (Abcam ab8898, 1:2000), Histone H3 (Cell Signaling 4499, 1:2000), KDM5A (Abcam 70892, 1:1000), KDM6A (Cell Signaling 33510, 1:1000), KDM6B (Abcam 38113, 1:1000), MyHC (Sigma MY32, 1:5000), MYC (Cell Signaling 5605, 1:1000), Tubulin (Sigma T5168, 1:5000), and Vinculin (Sigma V9131, 1:5000). HRP-conjugated secondary antibodies (Pierce, 1:5000) targeting the primary antibodies were detected with and chemiluminescent HRP substrates (Supersignal West Pico, Thermo Fisher Scientific; Supersignal West Femto, Thermo Fisher Scientific; or Immobilon, Millipore).

Metabolite Profiling

To measure changes in intracellular metabolite levels, cells were seeded in 6-well plates in their respective growth or differentiation media, as appropriate. To isolate metabolites the

cells were placed on ice and the cell culture was removed by aspiration. The cells were then washed twice with ice cold saline and snap frozen by floating the cell culture plates on liquid Nitrogen. To extract metabolites, frozen cells from each well were scraped in 400 µl of 75% Methanol and transferred into fresh Eppendorf tubes. 300 µl of Chloroform was then added and vortexed at 4°C for 20 min. Samples were centrifuged at 16.2K rcf for 10 min at 4°C on an Eppendorf 5415R tabletop centrifuge and 200 µl of the aqueous (top) layer was collected and dried overnight at 4°C in a CentriVap vacuum concentrator (Labonco). Dried samples were derivatized by first resuspending in 20 µl Methoxamine (MOX) and incubating for 60 min at 37°C, followed by the addition of 30 µl N-tert-butyldimethylsilyl-N-methyltrifluoroacetamide (TBDMS) and incubation for 90 min at 65°C. Derivatized metabolites were analyzed on an Agilent 7890B GC/5977A MSD system.

Enantiomer-specific 2-HG measurements were performed by LC-MS using a modified version of a previously published method (*40*). Cell lysates were extracted in a mixture of 75% methanol and chloroform spiked with 0.1 µg/ml of racemic mixture of $^{13}C_5$-2HG as an internal standard, and dried overnight at 4°C in a CentriVap vacuum concentrator (as described in detail above). Metabolites were resuspended in 100 µl of 50 mg/ml diacetyl-L-tartaric anhydride (DATAN, Sigma 358924) prepared fresh in a solution of dichloromethane (Sigma 650463) and acetic acid (Sigma 45754) [v/v = 4:1] and derivatized at 70°C for 2 hours. Derivatized samples were dried in a speedvac for 1 hour, resuspended in 50 µl of UltraPure water (18.2 MΩ, PureLab), and clarified by centrifugation at 4°C. 5 µl was analyzed by LC–MS/MS.

Chromatographic separation was performed using an Agilent Infinity 1290 II LC system, and detection was performed using an Agilent 6470 triple-quadrupole mass spectrometer operating in MRM and negative ion modes with Jet Stream source. Samples were ionized with

the following MS source parameters: nebulizer = 45 psi, capillary voltage = 2000 V, nozzle voltage = 500 V, sheath gas temperature = 325°C, sheath gas flow = 12 L/min., gas flow = 13 L/min., and gas temperature = 150°C. The fragmentor energy was set at 70 V and the cell accelerator voltage was set at 4 V for all compounds. MRM transitions were monitored for DATAN-derivatized compounds using the following parent ion, fragment ions, and collision energies (CE), with the primary transition for ion quantification indicated using an asterisk: $^{13}C_5$-2HG m/z 368 → 134* (CE = 29 V) and m/z 360 → 152 (CE = 5 V), 2HG m/z 363 → 129* (CE = 29 V) and m/z 363 → 147 (CE = 5 V), malate m/z 349 → 133* (CE = 14 V) and m/z 349 → 115 (CE = 28 V), and lactate m/z 305 → 89.1 (CE = 14 V).

Enantiomer identities were assigned using the retention time for the ^{13}C-labeled internal standard added to each sample. Chromatograms were analyzed using Agilent MassHunter Quantitative Analysis (for QQQ) software.

For quantification of absolute levels of intracellular 2-HG by GC-MS, total ion counts measured from the respective samples was quantified against a standard curve of L-2HG in water. Absolute levels of enantiomer-specific 2-HG were calculated either by normalizing the peak area measured by LC-MS either against an external standard curve prepared in the same cellular matrix or using the peak areas recorded for the $^{13}C_5$-2HG internal standard. Pilot experiments confirmed no measurable difference in quantifications obtained using either approach. For both GC-MS and LC-MS based approaches, we assumed that all suspended cells were perfect spheres. Cell counts and average cell diameter in each well were used to define the total intracellular volume {Volume = [πx(Average Cellular Diameter)^3]/6}, thus allowing for an absolute quantification of intracellular 2-HG concentration per well.

Baculoviral Protein Expression and Purification

Recombinant proteins were produced by transducing *Sf9* insect cells with the corresponding baculoviruses for 72 h. The cells were then washed with cold 1X PBS, and homogenized in a buffer containing 10 mM Tris-HCl pH 7.8, 150 mM NaCl, 100 mM glycine, 5 μM $FeSO_4$, 0.1% Triton X-100 and PIC. The soluble fractions of the FLAG-tagged enzymes were affinity purified using the anti-FLAG M2 affinity gel (Sigma), washed with TBS containing 5 μM $FeSO_4$ and PIC, and eluted with 150 µg/ml FLAG-peptide. KDM6B (1164→End) was further purified using UNOQ1 anion exchange column (Bio-Rad) to eliminate nucleic acid contamination. KDM6B was bound to the column in the FLAG affinity gel elution buffer and eluted with a gradient from 0 to 1 M NaCl in 50 mM Tris-HCl [pH 7.6]. For His-tagged KDM4A and KDM4B, the soluble fractions were affinity purified using Ni-NTA agarose (Qiagen) and eluted with imidazole, which was then removed with PD-10 columns (Sigma).The fractions collected were analyzed using 10% SDS-PAGE under reducing conditions followed by Coomassie Blue staining.

Circular dichroism (CD) spectroscopy

CD spectroscopy was performed using a Chirascan CD spectrometer (Applied Photophysics, Leatherhead, UK). CD data were collected between 190 and 260 nm at 22°C using a 1 cm path-length quartz cuvette. CD measurements were acquired every 1 nm with 1 s as an integration time and repeated three times with baseline correction. The data were analyzed with Pro-Data Viewer (Applied Photophysics).

Determination of melting temperatures

Thermal unfolding of wild-type and MT/ET KDM6A were recorded between 210 and 260 nm from 22°C to 94°C with a 2°C step size at 1°C/min ramp rate with ± 0.2°C tolerance. The melting temperatures were analyzed with Global3 (Applied Photophysics).

Enzyme kinetic assays

Oxygen K_m values for the KDMs were measured using a modified version of a previously described assays (*41, 42*), based on the stoichiometric coupling of lysine demethylation to 2-OG decarboxylation. Each 50 µl reaction volume consisted of 50 mM Tris-HCl [pH 7.8] (except for KDM5A, which was in MES [pH 6.5], and KDM5C and KDM5D, which were in Tris-HCl [pH 7.5]), 2 mg/ml bovine serum albumin (Roche), 60 µg/ml catalase (Sigma), 0.1 mM dithiothreitol, 2 mM sodium ascorbate, 50 µM iron(II) sulfate, 10% (v/v) dimethyl sulfoxide, and 50 µM (KDM4A and KDM4B), 40 µM (KDM5A, KDM5C and KDM5D), or 200 µM (KDM5B, KDM6A and KDM6B) of 2-oxo[1-^{14}C]glutarate (Perkin-Elmer). Respective histone peptides were used as substrates at saturating concentrations. These were 200 µM and 500 µM histone H3(1-19)K9me3 (Innovagen) for KDM4A and KDM4B, respectively, 30 µM (KDM5A), 20 µM (KDM5B), 15 µM (KDM5C and KDM5D) histone H3(1-21)K4me3 (Anaspec or Innovagen), respectively , and 1000 µM and 100 µM histone H3(21-44)K27(me3) (Innovagen) for KDM6A and KDM6B, respectively. All peptide substrates contained an additional glycine and a biotinylated lysine residue at their C-termini. Enzyme concentrations were 0.2-1.5 µM. Enzymatic reactions were simultaneously performed in five to six different oxygen concentration using an InVivo400 hypoxia workstation (Ruskinn), following an initial reagent equilibration at

the corresponding oxygen concentration. The reaction endpoints, chosen within the linear phase of the enzymatic assay time curves (*15*) and Fig. S7), were the following: KDM4A, KDM4B, KDM5B, KDM6A and KDM6A (931→End) 20 min, KDM6B (1164→End) 15 min, Fig KDM5A, KDM5C, KDM5D and KDM6B 3 min. Reactions were stopped by adding 100 µl of 1M potassium phosphate pH 5 and the amount of ^{14}C-labeled CO_2 generated was scintillated in a Tri-Carb 2900TR (Perkin Elmer). When the effect of H_2O_2 on the catalytic activity of KDM6A and the MT/ED mutant was studied catalase was omitted from the reaction. K_M values were determined from the Michaelis-Menten saturation curves and Lineweaver-Burk plots using Microsoft Excel. V_{max} values for wild type KDM6A and the KDM6A MT/ED mutant were calculated from the Michaelis-Menten saturation curves and Lineweaver-Burk plots using Microsoft Excel after standardizing observed d.p.m. values for enzyme amount quantified from the Coomassie Blue-stained SDS-PAGE gel. L-2HG IC_{50} values for wild-type and MT/ED KDM6A were determined by increasing the concentration of L-2HG in the presence of non-limiting amounts of other factors, and in the presence of 37.5 µM 2-oxoglutarate.

Myogenic Differentiation Assays

C2C12 cells were seeded in 6-well plates in growth medium [DMEM, 10% FBS, and 1X Penicillin/Streptomycin] at a density of 200,000 cells/well and allowed to adhere overnight at 37°C. Differentiation was induced for 4 days by switching cells into differentiation media [DM: DMEM, 2% Horse serum, 1X insulin-transferrin-selenium (ITS)] supplemented with 1X Penicillin/Streptomycin on day 0, followed by media changes on day 2 and day 3. For Metformin rescue experiments, cells were seeded in growth medium in the presence of the indicated

concentrations of Metformin, and Metformin treatment was continued in differentiation medium throughout the course of the experiment.

Mouse Embryonic Fibroblasts lentivirally transduced to express a MyoD-ER fusion were cultured and seeded (as described above) in growth medium [DMEM, 10% FBS] supplemented with 1X Penicillin/Streptomycin and then induced to differentiate by being switched to DM using the schema described in fig. S13.

Differentiation assays were scored by measuring the mRNA levels of myogenic differentiation markers by Real-Time qPCR and by scoring "Fusion Index (FI)". FI was measured by counting multi-nucleated MyHC positive myotubes from 3 representative fields (~350 cells/field) from each biological replicate. Mean FI +/- SD from 3 biological replicates was compared by statistical analysis.

Human Skeletal Myoblasts were seeded at a density of 300,000 cells per well of a 6-well plate in Skeletal Muscle Growth Medium (ZenBio, SKM-M) and allowed to adhere overnight at 37°C. Differentiation was induced in DM for 3-4 days with daily media changes.

Immunofluorescence staining

For immunofluorescence assays, C2C12 cells were seeded on coverslips and cultured in 6-well plates under the desired conditions. To fix cells, the media was aspirated and cells were washed twice with cold 1X PBS, and fixed using 2% formaldehyde in 1X PBS for 15 minutes at room temperature. Cells were permeabilized on ice for 5 mins using 0.5% TritonX-100 in 1X PBS and then blocked for 10 minutes using blocking buffer [5% normal goat serum (NGS) in 1X PBS]. Cells were stained sequentially with primary and secondary antibody diluted in wash buffer [1% normal goat serum (NGS) in 1X PBS] for 1 hour each at room temperature. Cells

were washed thrice after both primary and secondary antibody staining. The cells were then counterstained with DAPI and mounted onto slides using mounting medium. Stained cells were imaged using a Nikon inverted TE2000 inverted fluorescence microscope equipped with a motorized platform and a Hamamatsu Orca ER digital CCD camera and analyzed using ImageJ.

Immunohistochemistry

For immunohistochemistry analyses, 4 um thick paraffin-embedded tissue sections were prepared and left to air-dry overnight. Slides were baked in an Isotemp Oven (Fisher Scientific) for 30 minutes at 60°C to melt excess paraffin. Immunohistochemical staining for H3K27me3 was performed on a Bond III automated stainer (Leica Biosystems) using the Bond Polymer Refine Detection Kit (Leica Biosystems cat. no. DS9800). Briefly, antigen retrieval was performed using the Bond Epitope Retrieval Solution 1 (Citrate, pH 6.0) for 30 minutes, following which slides were incubated with a rabbit monoclonal antibody directed against H3K27me3 (Cell Signaling Technology cat. no. 9733, 1:200) diluted in Bond Primary Antibody Diluent (Leica Biosystems cat. no. AR9352) for 30 minutes. Slides were subsequently incubated with the HRP-conjugated secondary antibody for 10 minutes. Staining was visualized by incubating the slides with the chromogen 3,3'-diaminobenzidine for 5 minutes. Finally, slides were counterstained with hematoxylin, dehydrated in graded ethanol and xylene, and cover-slipped. Typically 3 serial sections from 2 male and 2 female mice (for main figure 1G) and 5 independent tumors (for fig. S10) were stained and analyzed.

Flow cytometry analysis

Flow cytometry analysis for intracellular Myosin Heavy Chain expression was performed on cells fixed for 15 minutes with 1% Formaldehyde at room temperature. Cells were permeabilized on ice for 10 mins using 0.5% TritonX-100 in 1X PBS and then blocked for 30 minutes in blocking buffer. Cells were stained with primary antibody (APC-conjugated anti-MyHC, R&D Biosystems) for 3 hours at room temperature in the dark. For intracellular ROS measurements, cells were cultured for 2 hours in the presence of deep red CellROX (Invitrogen), as per the manufacturer's instructions. The cells were then harvested using trypsin and resuspended in growth medium. For CD44 staining, HMLE cells fixed as above were washed once in ice-cold PBS and resuspended in 50 µl of staining solution [5 µl AlexaFluor 700 conjugated anti-CD44 (BD 561289), 1% FBS, in 1X PBS] and incubated at 25°C in the dark for 2 hours. For all measurements, cells were washed thrice, resuspended in wash buffer (1%FBS in 1X PBS), and then analyzed by flow cytometry using a BD LSR II system. In all flow based assays, measurements from 10,000 cells were collected for analysis and measurements from 1000 cells was displayed in the plots.

RNA-Seq and transcriptional analysis

RNA-Seq analysis was performed on total RNA extracted from cells using Trizol (Life Technologies) according to the manufacturer's instructions. Total RNA was sent to the Molecular Biology Core Facility (MBCF, Dana-Farber Cancer Institute) for library construction and sequencing. Libraries were prepared from 500ng of purified total RNA using Illumina Truseq Stranded mRNA samples preparation kits according to the manufacturer's protocol. Finished libraries were quantified by Qubit fluorometer, Agilent TapeStation 2200, and RT-qPCR using the Kapa Biosystems library quantification kit according to manufacturer's

protocols. Uniquely indexed libraries were pooled in equimolar ratios and sequenced on an Illumina NextSeq500 run with single-end 75bp reads.

Sequenced reads were aligned to the UCSC mm9 reference genome assembly and gene counts were quantified using STAR (v2.5.1b) (*43*) and normalized read counts (RPKM) were calculated using cufflinks (v2.2.1) (*44*). RNAseq analysis was performed using the VIPER snakemake pipeline (*45*).

ChIP-Seq Analysis

ChIP-Seq analysis was performed using C2C12 cells cultured under the desired conditions. Briefly, after aspirating culture medium, cells were washed with cold 1X PBS, and fixed using 1% formaldehyde (reconstituted in 1X PBS) at room temperature for 10 min. Excess formaldehyde was quenched by dropwise addition of Glycine to a final concentration 125 mM and further incubation at room temperature for 5 min. Fixed cells were harvested, washed 1X with cold 1X PBS, lysed in SDS buffer (50mM Tris-HCl [pH 8], 1% SDS, 10mM EDTA), and sonicated in the cold using a microprobe (5 cycles: 10" on/10" off). Lysates were clarified by centrifugation at 16.2K rcf for 10 min at 4°C. To test for sonication efficiency and quantify the concentration of chromatin, 20 µl of the clarified lysates was aliquoted into a fresh tube. Sample volume was adjusted to 100 µl using TE, and treated sequentially, first by addition of 1 µl RNAse (10 mg/ml, Roche) for 30 min at 37°C, followed by addition of 5 µl of Proteinase K (20 mg/ml) and incubation overnight at 65°C. DNA was recovered by column purification using a Qiagen kit, as per the manufacturer's instructions, run on a gel to ensure an average size of <500bp, and quantified on a Nanodrop.

ChIP was performed in a 1000-1500 µl reactions reconstituted in ChIP Dilution Buffer [20mM Tris-HCl pH 8, 1% Triton-X 100, 2mM EDTA, 150mM NaCl + PIC], diluting SDS Buffer at least 1:5 (ideally 1:10), and using 3 µg chromatin, 10 µl of anti-H3K27me3 (Cell Signaling), and 50 µl of blocked A/G beads.

Blocked A/G beads were prepared in advance by incubating 500 µl of 50% slurry (1:1 Protein A:Protein G beads) with 15 µl Sonicated Herring Sperm DNA (10 mg/ml) and 50 µl BSA (10 mg/ml), overnight at 4°C. Beads were washed thrice with 1 ml cold ChIP Dilution Buffer and re-adjusted to 50% slurry by addition of 250 µl of ChIP Dilution Buffer.

ChIPs were performed by tumbling down the reconstituted reactions for 3 hours are 4°C. Beads were washed thrice with ChIP Dilution Buffer and bound DNA was recovered from the beads by following the RNAse and ProteinaseK treatments, followed by purification over the Qiagen column, as described above. Recovered DNA was quantified by Qubit and used to prepare libraries using the Illumina Nextera library prep method. Samples were run on a NextSeq 500 and mapped and analysed using the ChiLin analytical pipeline (*46*). Genomic H3K27me3 recruitment was compared using the Integrated Genome Viewer (*47*).

ChIP-Seq reads generated from H3K4me3 and H3K27me3 libraries were aligned to the mouse genome (mm9) using bowtie2 (*48*) using the default options. Enrichment of the histone marks were calculated relative to input in 50-bp non-overlapping bins using the R package spp (*49*). Tag density was estimated using a Gaussian kernel with bandwidth of 35 as described in spp package. Standard BigWig files were generated for both tag enrichment and tag density for visualization in the genome browser. Reference transcript annotations for the mouse genome were obtained from the University of California Santa Cruz Genomics Institute (UCSC) (*50*). Mean histone enrichment was calculated within a -2Kb to +5Kb region relative to each

transcription start site (TSS). For gene bodies, mean histone enrichment was calculated from the start site of each transcript to the termination site. Mean histone enrichment was then compared to expression data produced by the VIPER package (*45*) and correlations were calculated using R. Gene ontology enrichment for H3K4me3 or H3K27me3 marked genes (normoxia versus hypoxia) was carried out from cells in differentiation media using PANTHER (*51, 52*), employing a TSS-proximal enrichment fold-change cutoff of >=2 and a significance cutoff of $p < 0.05$.

Gene Set Enrichment Analysis

Gene set enrichment analysis (GSEA) (*26*) was performed using TCGA data on gene sets in the Hallmark collection (MSigDB http://software.broadinstitute.org/gsea/msigdb) and curated gene sets related to H2K27me3 (Table. S2). Tumors that were previously annotated as "hypoxic" or "normoxic" based on HIF signature (*27*) (Table. S1), were analyzed from the TCGA cohorts BLCA, BRCA, COAD, HNSC, LUAD, LUSC, and UCEC. Standardized RSEM RNA-seq data was downloaded from the Broad Institute TCGA GDAC Firehose repository (*53*). Samples sequenced by Illumina Genome Analyzer and HiSeq machines were pooled and duplicate samples were removed.

GSEA parameters are as follows:

```
 --GSEA.v.1.0.reshuffling.type "sample.labels" \
 --GSEA.v.1.0.nperm 500 \
 --GSEA.v.1.0.weighted.score.type 1 \
 --GSEA.v.1.0.nom.p.val.threshold -1.0 \
```

--GSEA.v.1.0.fwer.p.val.threshold -1.0 \

--GSEA.v.1.0.fdr.q.val.threshold 0.25 \

--GSEA.v.1.0.topgs 20 \

--GSEA.v.1.0.adjust.FDR.q.val F \

--GSEA.v.1.0.gs.size.threshold.min 25 \

--GSEA.v.1.0.gs.size.threshold.max 500 \

--GSEA.v.1.0.reverse.sign F \

--GSEA.v.1.0.perm.type 0 \

Structural analyses

The crystal structure coordinates for KDM6A (PDB: 3avr) and KDM6B (PDB: 2xue) demethylase domains (*32, 33*) were downloaded from Protein Data Bank. The structures were aligned and a composite image of the active site was created in PyMOL. Atomic distances between residues lining the catalytic pocket were measured using PyMOL.

Statistical Analysis

All experimental results represent observations from at least 3 biological replicates, except for the genomics data (ChIP-Seq and RNA-Seq), which were measured from 2 biological replicates. All genomic analysis were performed in R using the "spp" package (*49*), as described in the methods. Unless indicated otherwise, all data are presented as mean +/- SD and the number of replicates is indicated in the legends. All statistical analysis were performed using the GraphPad Prism package. Statistical significance was calculated by *t-test*, assuming gaussian

distribution, unpaired with the Welch's correction, and values below 0.05 were considered significant. Multiple testing corrections, if necessary, were performed by the Holm-Sidak method using Graphpad Prism. For GSEA (*26*), as described in the algorithm's manual, a FDR (q) value below 0.25 was considered significant.

Primer/Oligos List

No.	Name	Sequence	Remarks
1	ARNT (*68*)F	ggggacaactttgtacaaaaaagttggcATGGCAGCGACTACTGCCAA	Primers used for gateway sub-cloning wild-type of mutant (414) ARNT into the pLX304 vectors
2	ARNTΔ414(*68*)F	ggggacaactttgtacaaaaaagttggcATGAAGTCCTTGCGGGGAAC	
3	ARNT (*68*)R	ggggacaactttgtacaagaaagttgggcaTTCTGAAAAGGGGGGAAACAT	
4	mNdrg1_F	ATGTCCCGAGAGCTACATGA	Primers used for Real-Time qPCR analysis
5	mNdrg1_R	TGACATGCAGGGAGCCATGT	
6	mAdm_F	CCTTCGCAGTTCCGAAAGAA	
7	mAdm_R	AGTTGTGTTCTGCTCGTCCA	
8	mEgln3_F	CTATGTCAAGGAGCGGTCCAA	
9	mEgln3_R	GTCCACATGGCGAACATAACC	
10	mKDM6A_F	TACGAATCTCTAATCTTAAA	
11	mKDM6A_R	TTCCAGTAATCAGACTGTAA	
12	mKDM6B_F	CCTGCAGTCAATGAAGCACTG	
13	mKDM6B_R	CTCCACGTCGCATTCGTTG	
14	ExoUTX_F	TTGATCTGCTTTTTGTCACT	
15	ExoUTX_R	ACCGAGGAGAGGGTTAGGGAT	
16	mActin_F	TAGGCACCAGGGTGTGATG	
17	mActin_R	CATGGCTGGGGTGTTGAAGG	

18	6Asg1Top	CACCGTCCTTGGCTCGACAAAAGCT	Oligos used to generate sgRNAs targeting *Kdm6a*
19	6Asg1Btm	AAACAGCTTTTGTCGAGCCAAGGAC	
20	6Asg2Top	CACCGCCGCCTTTTCGGGTTCGTG	
21	6Asg2Btm	AAACCACGAACCCGAAAAGGCGGC	
22	ARNTsg1Top	CACCGGGCTATTAAGCGACGGTCA	Oligos used to generate sgRNAs targeting *Arnt*
23	ARNTsg1Btm	AAACTGACCGTCGCTTAATAGCCC	
24	ARNTsg2Top	CACCGAGAAACGGCCATGCGTAAGA	
25	ARNTsg2Btm	AAACTCTTACGCATGGCCGTTTCTC	
26	EZH2sg1Top	CACCGCGGCCCCCTGGGCGTTTAGG	Oligos used to generate sgRNAs targeting *EZH2*
27	EZH2sg1Btm	AAACCCTAAACGCCCAGGGGGCCGC	
28	EZH2sg2Top	CACCGAATAACTGCACTTACGATGT	
29	EZH2sg2Btm	AAACACATCGTAAGTGCAGTTATTC	
30	6A_MT_Top	Aatttgaatttcctaacgggttcttggtggcccaa	Oligos used for site-directed mutagenesis of KDM6A cDNA
31	6A_MT_Btm	ttgggccaccaagaacccgttaggaaattcaaatt	
32	6A_ED_Top	tactgtagcatttgtgatgtggaggtttttgat	
33	6A_ED_Btm	atcaaaaacctccacatcacaaatgctacagta	

34	6Bsg1Top	CACCGAAGCTTCCTCCATAGC GAA	Oligos used to generate sgRNAs targeting *Kdm6b*
35	6Bsg1Btm	AAACTTCGCTATGGAGGAAG CTTC	
36	6Bsg2Top	CACCGCTGCAAGCGGCCAATC CG	
37	6Bsg2Btm	AAACCGGATTGGCCGCTTGCA GC	
38	Hu6Asg1Top	CACCGCAGCATTATCTGCATA CCAG	Oligos used to generate sgRNAs targeting *KDM6A*
39	Hu6Asg1Btm	AAACCTGGTATGCAGATAATG CTGC	
40	Hu6Asg2Top	CACCGTTGGATAATCTTCCAA TAAG	
41	Hu6Asg2Btm	AAACCTTATTGGAAGATTATC CAAC	
42	mKdm5A sg1top	CACCGTCTTTGAGCCCAGTTG GG	Oligos used to generate sgRNAs targeting *Kdm5a*
43	mKdm5A sg1btm	AAACCCCAACTGGGCTCAAA GAC	

44	mKdm5A sg2top	CACCGGCGCCCGATAAAACTCAG	
45	mKdm5A sg2btm	AAACCTGAGTTTTATCGGGCGCC	
46	L2HGDHsg1top	CACCGAAAGAAGGAGCCGTATTGCA	Oligos used to generate sgRNAs targeting *L2hgdh*
47	L2HGDHsg1btm	AAACTGCAATACGGCTCCTTCTTTC	
48	L2HGDHsg2top	CACCGACCTCAAGGGAATTCCCTAC	
49	L2HGDHsg2btm	AAACGTAGGGAATTCCCTTGAGGTC	
50	L2HGDHsg3top	CACCGAAACATCCTGGACTTTCGAT	
51	L2HGDHsg3btm	AAACATCGAAAGTCCAGGATGTTTC	
52	L2HGDHsg4top	CACCGTCTTTTGATATAGTCATCGT	
53	L2HGDHsg4btm	AAACACGATGACTATATCAAAAGAC	
54	hKRT14_F	TGAGCCGCATTCTGAACGAG	Primers used for Real-Time qPCR analysis
55	hKRT14_R	GATGACTGCGATCCAGAGGA	
56	hZEB1_F	CAGCTTGATACCTGTGAATGGG	
57	hZEB1_R	TATCTGTGGTCGTGTGGGACT	
58	mMyl1_F	AAGATCGAGTTCTCTAAGGAGCA	
59	mMyl1_R	TCATGGGCAGAAACTGTTCAAA	
60	mMyog_F	GAGACATCCCCCTATTTCTACCA	
61	mMyog_R	GCTCAGTCCGCTCATAGCC	

62	mMyl4_F	AAGAAACCCGAGCCTAAGAAGG	
63	mMyl4_R	TGGGTCAAAGGCAGAGTCCT	
64	mActc1_F	CTGGATTCTGGCGATGGTGTA	
65	mActc1_R	CGGACAATTTCACGTTCAGCA	
66	hACTC1_F	TCCCATCGAGCATGGTATCAT	
67	hACTC1_R	GGTACGGCCAGAAGCATACA	
68	hMYL1_F	GTTGAGGGTCTGCGTGTCTTT	
69	hMYL1_R	ACCCAGGGTGGCTAGAAC	

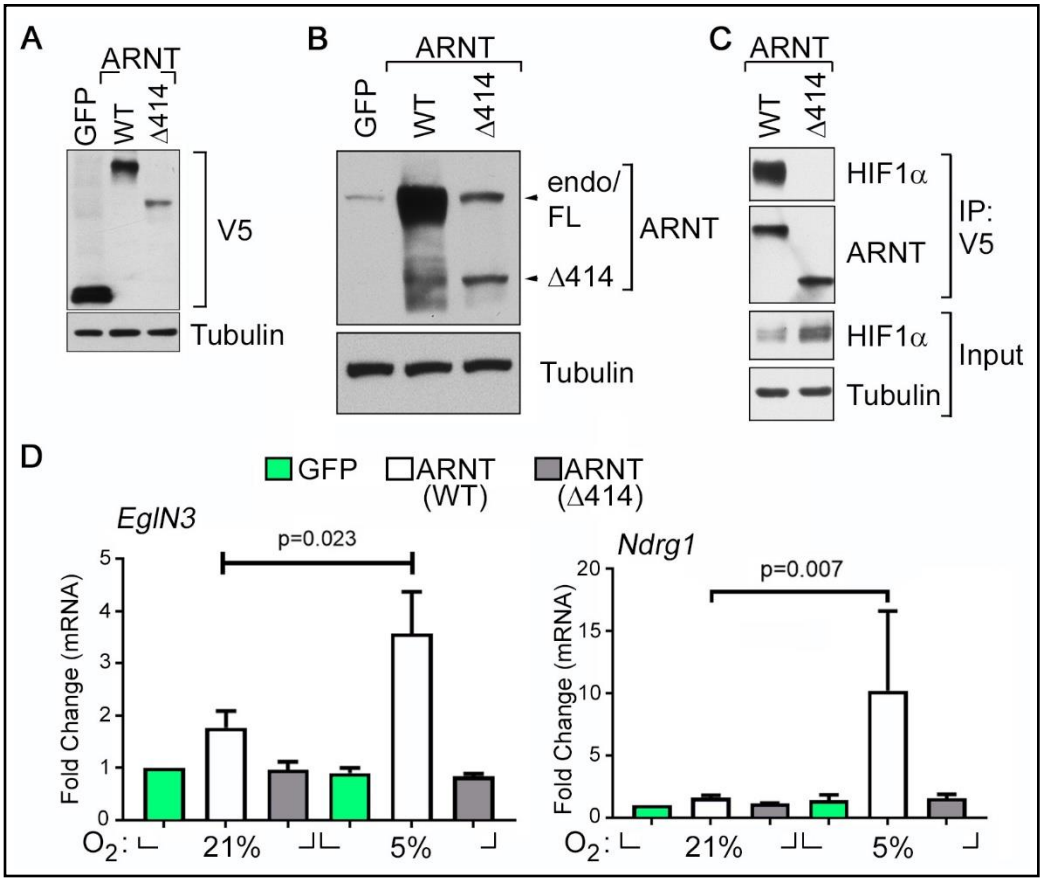

Fig. S1. Re-Expression of Wild-Type ARNT Restores HIF Activity in *Arnt*-deficient mHepa-1 c4 Cells.

(**A**-**B**) Anti-V5 (**A**) and Anti-ARNT (**B**) immunoblot analysis of *Arnt*-deficient mHepa-1 c4 cells that were lentivirally transduced to produce V5-tagged indicated isoforms of ARNT or GFP (as a control) and cultured in 21% oxygen. In (**B**) FL = full-length. endo = endogenous. mHepa-1 c4 cells express a defective version of ARNT in which glycine 326 is replaced with aspartic acid (*54*). (**C**) Immunoblot analysis of anti-V5 immunoprecipitates from cell lysates of mHepa-1 c4 cells that express either wild-type or Δ414 ARNT cultured in the presence of 1 μM MLN for 24 hours. MLN was added to promote the accumulation of HIF1α. (**D**) Real-Time qPCR analysis to

measure the abundance of the indicated genes in cells as in (**A**) that were cultured at the indicated oxygen concentration for 24 hours. Data represent mean +/- SD (*N*=3) and *p*-value was calculated using the Students *t*-test.

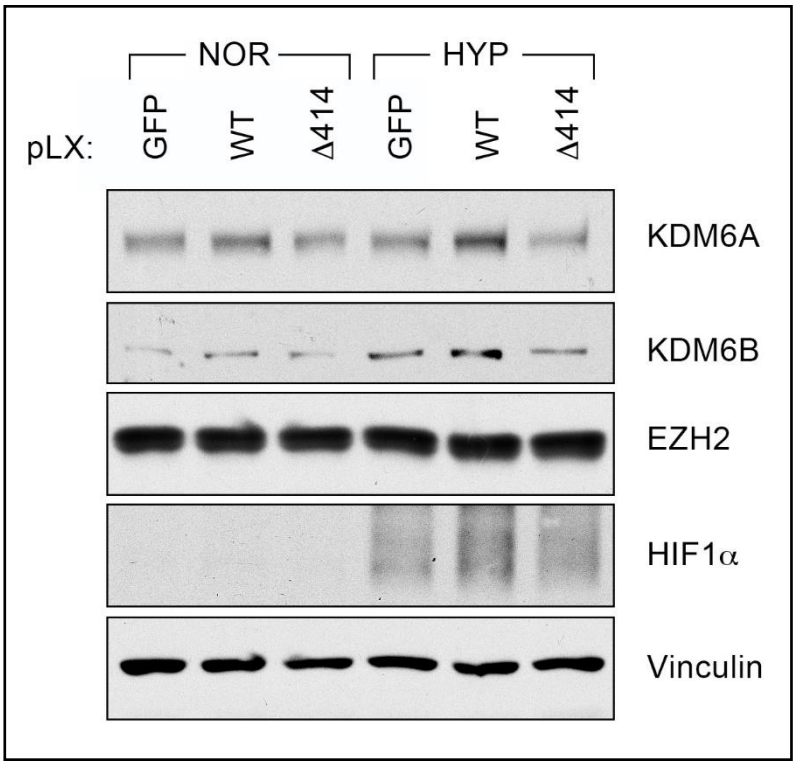

Fig. S2. Expression Levels of H3K27 Modifiers in mHepa-1 c4 Cells

Immunoblot analysis of mHepa-1 c4 cells that were lentivirally transduced to express the indicated ARNT isoforms or GFP (control) and cultured in 21% oxygen (NOR) or 5% oxygen (HYP), as indicated, for 2 days.

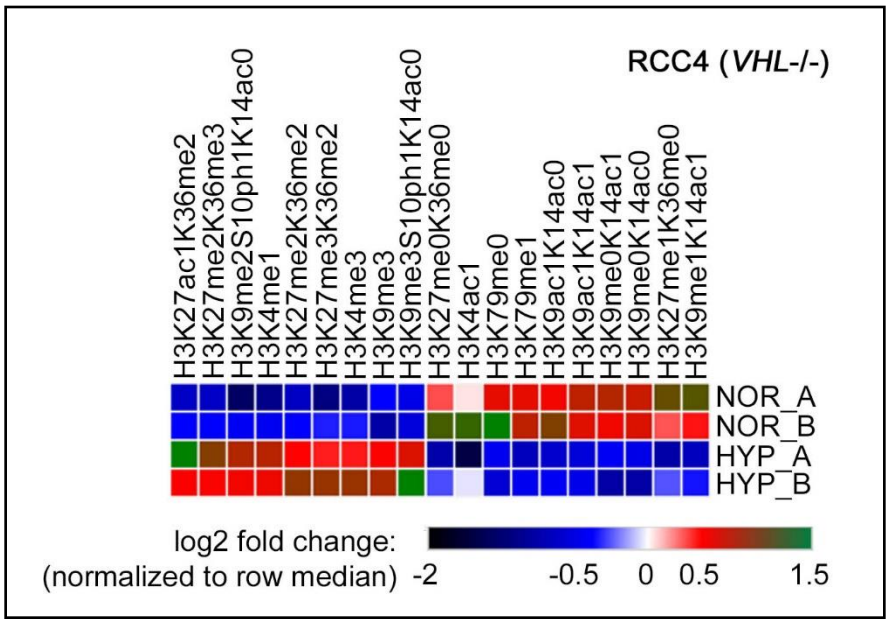

Fig. S3. Hypoxia Induces Histone Hypermethylation in *VHL*-deficient Renal Cells.

Histone modification profiling of 2 biological replicates (A and B) of *VHL*-deficient RCC4 cells that were either cultured in 21% oxygen (NOR) or in 1% oxygen (HYP) for 3 days. The color in each cell represents the $\log_2$ fold change relative to all other samples in the column after first normalizing total histone to an internal control peptide (Histone H3: residues 41-49).

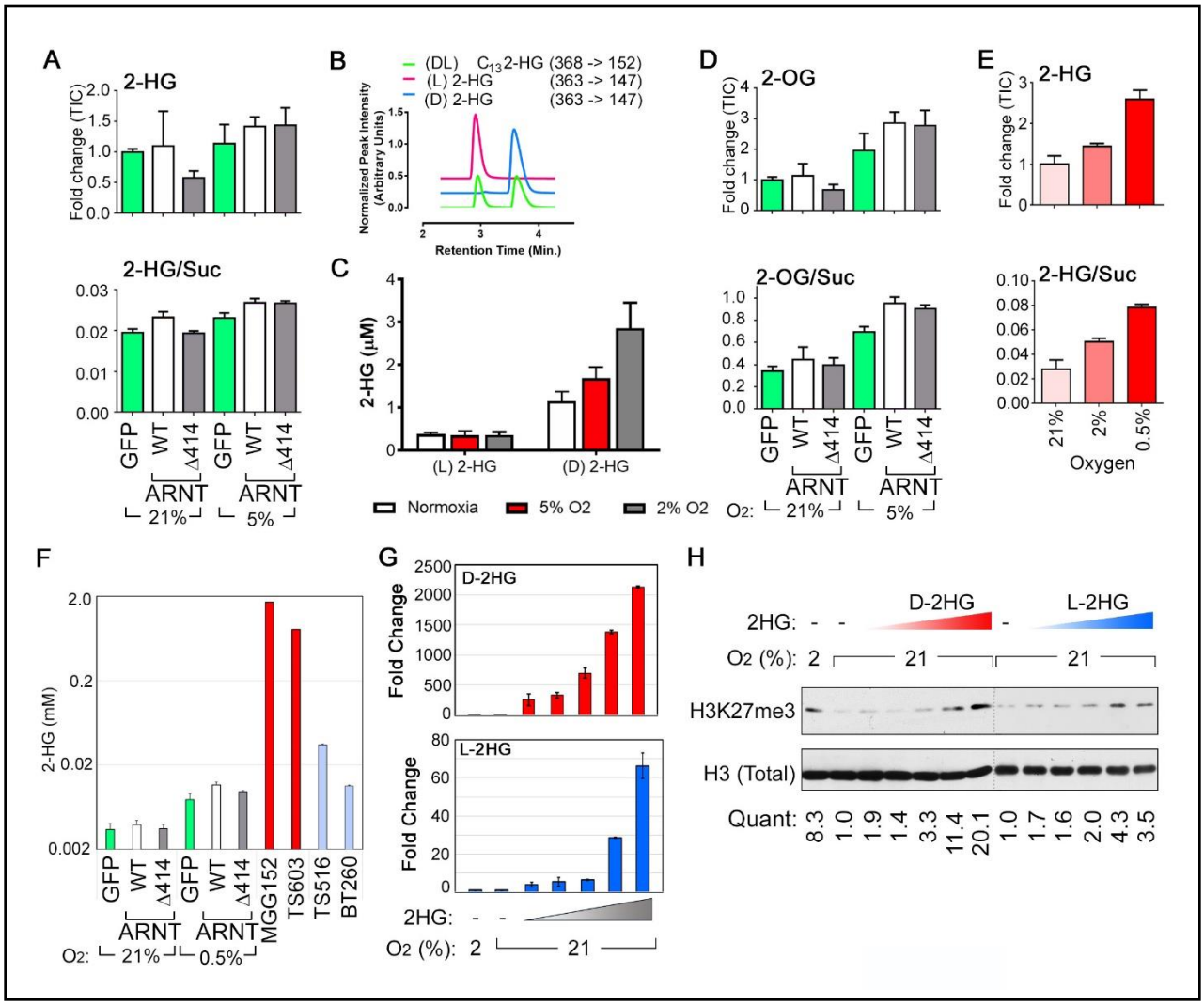

Fig. S4. Increased Histone Methylation Observed After Exposure to Modest Hypoxia is Not Caused by 2-HG.

(**A**) Intracellular levels of total 2-Hydroxyglutarate [2-HG] (**A**), as measured by GC-MS, in mHepa-1 c4 cells that were lentivirally transduced to produce the indicated ARNT isoforms or GFP (as a control) and cultured at the indicated oxygen concentrations for 4 days. Metabolite levels are represented either as fold changes in Total Ion Counts [TIC] [*top panel*] or as a ratio normalized to Succinate [Suc] levels [*bottom panel*]. Data represent mean +/- SD (*N*=4). (**B**-**C**)

LC-MS analysis of a racemic mixture or individual enantiomers of 2-HG standards in mHepa-1 c4 cell matrix (**B**) and absolute intracellular 2-HG concentrations in parental Hepa-1 c4 cells grown at the indicated oxygen concentrations for 4 days (**C**). In (**C**), data represents mean +/- SD (*N*=3). (**D**) Intracellular levels of 2-oxoglutarate [2-OG] measured by GC-MS, as in (**A**). Data represents mean +/- SD (*N*=4). (**E**) Total 2-Hydroxyglutarate [2-HG], as measured by GC-MS, in *ARNT*-deficient mHepa-1 c4 cells that were cultured at the indicated oxygen concentrations for 4 days. Metabolite levels are represented either as fold changes in Total Ion Counts [TIC] [*top panel*] or as a ratio normalized to Succinate [Suc] levels [*bottom panel*]. Data represents mean +/- SD (*N*=4). (**F**) Absolute quantification of intracellular levels of 2-HG in the mHepa-1 c4 cells as in (**A**), cultured at the indicated oxygen concentrations for 4 days. IDH1 wild type [TS516 and BT260] or IDH1 mutant [MGG152 and TS603] glioma cell lines were included for comparison (*37-39*). Note use of log scale for y-axis. (**G**) Fold change in 2-HG relative to basal normoxic levels (set to 1) in parental mHepa-1 c4 cells that were cultured for 48 hours in the presence of increasing concentrations of esterified D-2HG (top panel) or L-2HG (bottom panel). Media was replaced every 24 hours and analysis was performed on cell lysates collected 3 hours after the last media change. Triangle represents a 3-fold serial dilution series ranging from 0, 19, 56, 167, 500, and 1500 μM concentration of the indicated enantiomer. Note that despite using identical concentrations for both enantiomers, the levels of intracellular D-2HG achieved was orders of magnitude higher than L-2HG, perhaps indicating differences in catabolic activity. Data represents mean +/- SD (*N*=3). (**H**) Immunoblot analysis of mHepa-1 c4 cells cultured at the indicated oxygen concentrations in the presence or absence of esterified 2-HG for 48 hours, as in (**G**). "Quant" represents fold-change in densitometric ratios of H3K27me3 (normalized to total H3) relative to untreated normoxic cells.

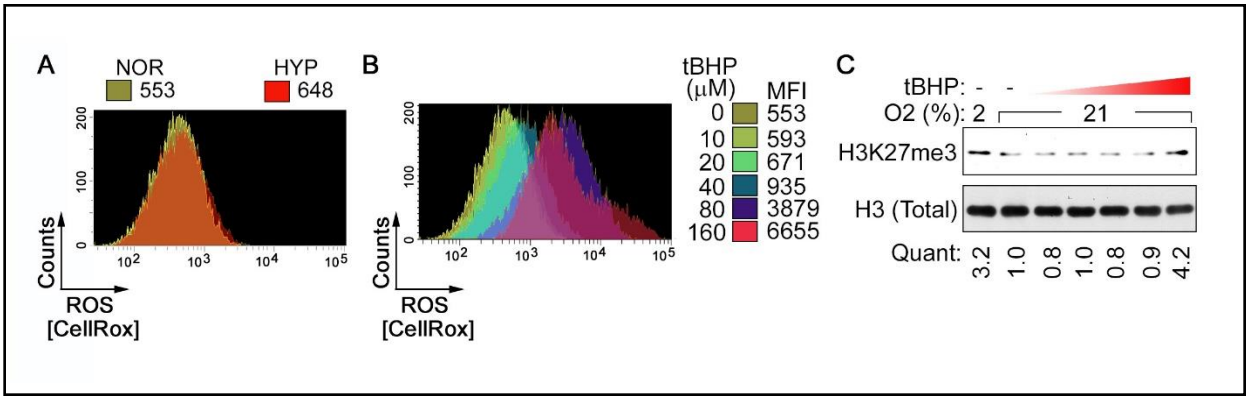

Fig. S5. ROS Induction Does Not Account for the Effects of Hypoxia on Histone Hypermethylation.

(**A** and **B**) Intracellular ROS levels, as measured by flow cytometry, in mHepa-1 c4 cells stained with the CellROX Deep Red reagent. (**A**) Comparison of cells cultured in 21% oxygen [NOR] or 2% oxygen [HYP], with values indicating Mean Fluorescence Index (MFI). (**B**) Comparison of intracellular ROS levels in cells treated with the indicated concentrations of tert-Butyl hydroperoxide (tBHP). The "tBHP=0" curve is identical to the "NOR" curve in (**A**) and is replicated for reference. (**C**) Immunoblot analysis of histones prepared from mHepa-1 c4 cells cultured at the indicated oxygen levels for 36 hours in the presence or absence of tBHP. Triangle represents a 2-fold serial dilution range of 10, 20, 40, 80, and 160 μM tBHP. "Quant" represents fold-change in densitometric ratios of H3K27me3 (normalized to total H3) relative to untreated normoxic cells.

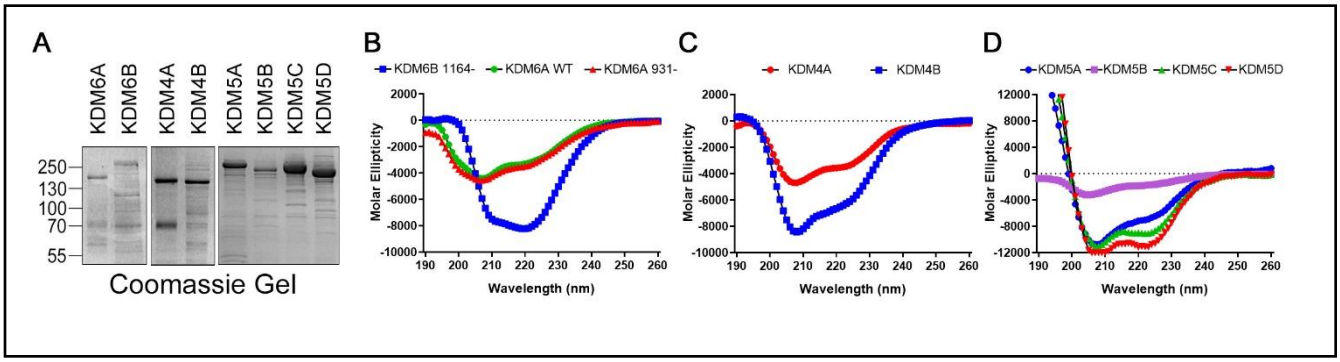

Fig. S6. Purification of Recombinant Histone Demethylases.

(**A**) Coomassie Blue dye staining of either His- or FLAG-tagged versions of the indicated histone demethylases that were expressed and affinity purified from baculovirally infected *Sf9* insect cells. "KDM6A 931-" = KDM6A*. "KDM6B 1164-" = KDM6B*. (see text) (**B**) Circular Dichroism (CD) data that were collected between 190 and 260 nm at 22°C. Measurements were acquired every 1 nm with 1 s as an integration time and repeated three times with baseline correction.

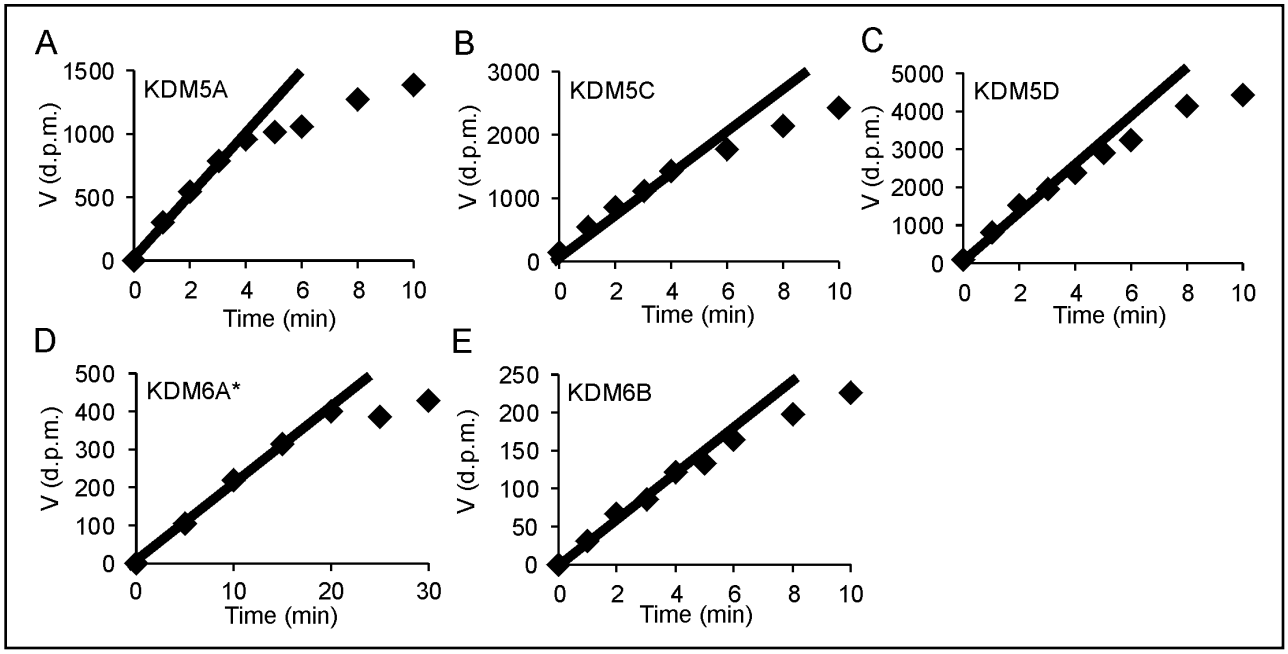

Fig. S7. Time Course Analysis of Recombinant Purified Histone Demethylases.

(**A**-**E**) The catalytic activity of the indicated recombinantly expressed and purified KDMs, as described in fig. S6, was studied with respect to time. The catalytic activity of KDM4A, KDM4B, KDM5B, KDM6A, and KDM6B* has been published earlier (*15*). * indicates the shortened version containing the JmjC domain.

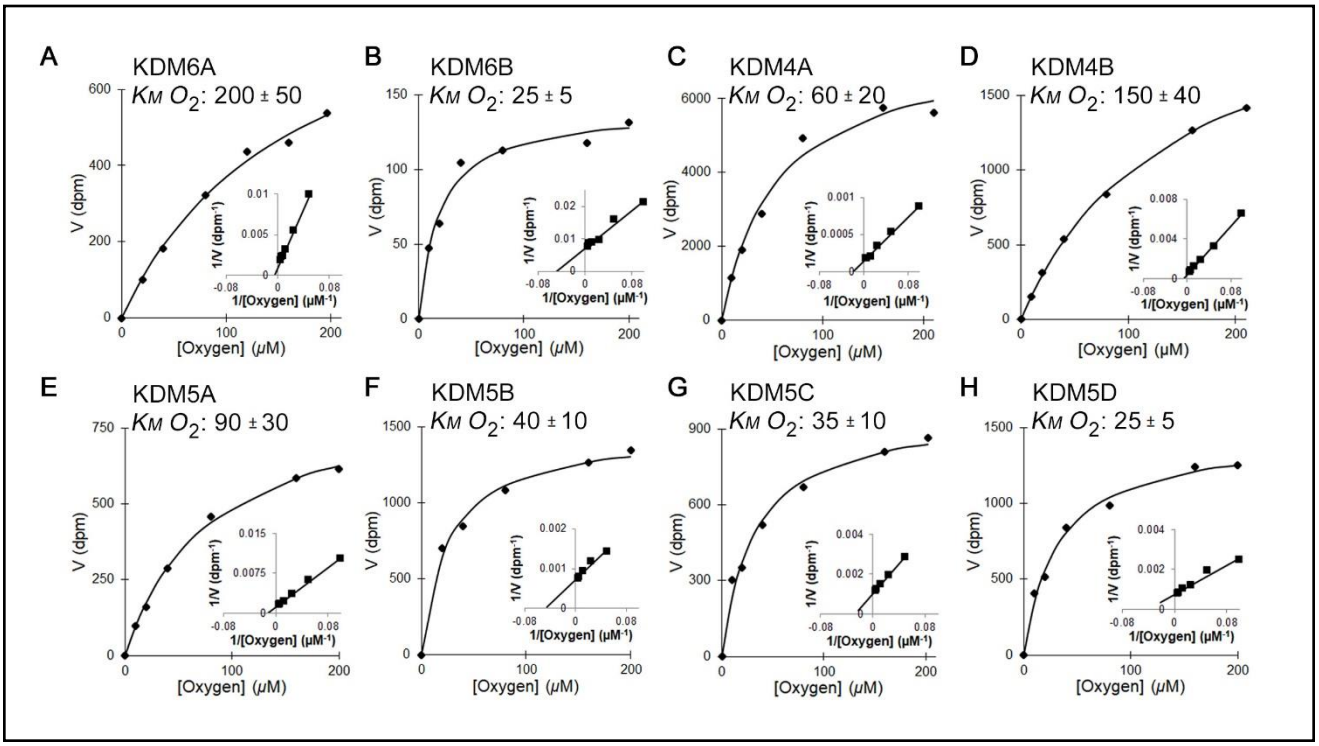

Fig. S8. Biochemical Characterization of Recombinant Purified Histone Demethylases.

(**A-H**) Representative Michaelis-Menten curves and Lineweaver-Burk plots [*insets*] showing the kinetic properties of the indicated baculovirally purified recombinant full length Histone Demethylases, measured over the indicated range of oxygen concentrations. K_M values in μM are depicted as mean +/- SD (*N*=3-12 independent measurements).

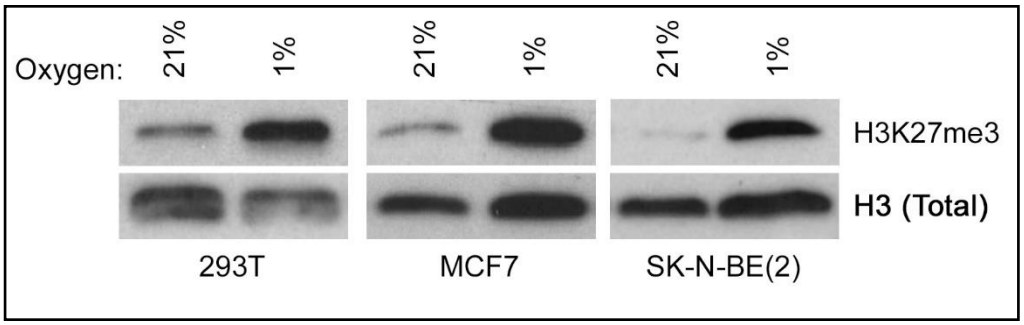

Fig. S9. Hypoxia Induces Histone Hypermethylation in pVHL-proficient Cell Lines.

Immunoblot analysis of histone lysates generated from the indicated cell lines cultured at the indicated oxygen concentrations for either 24 hours (MCF7 cells) or 72 hours (293T and SK-N-NE(2) cells).

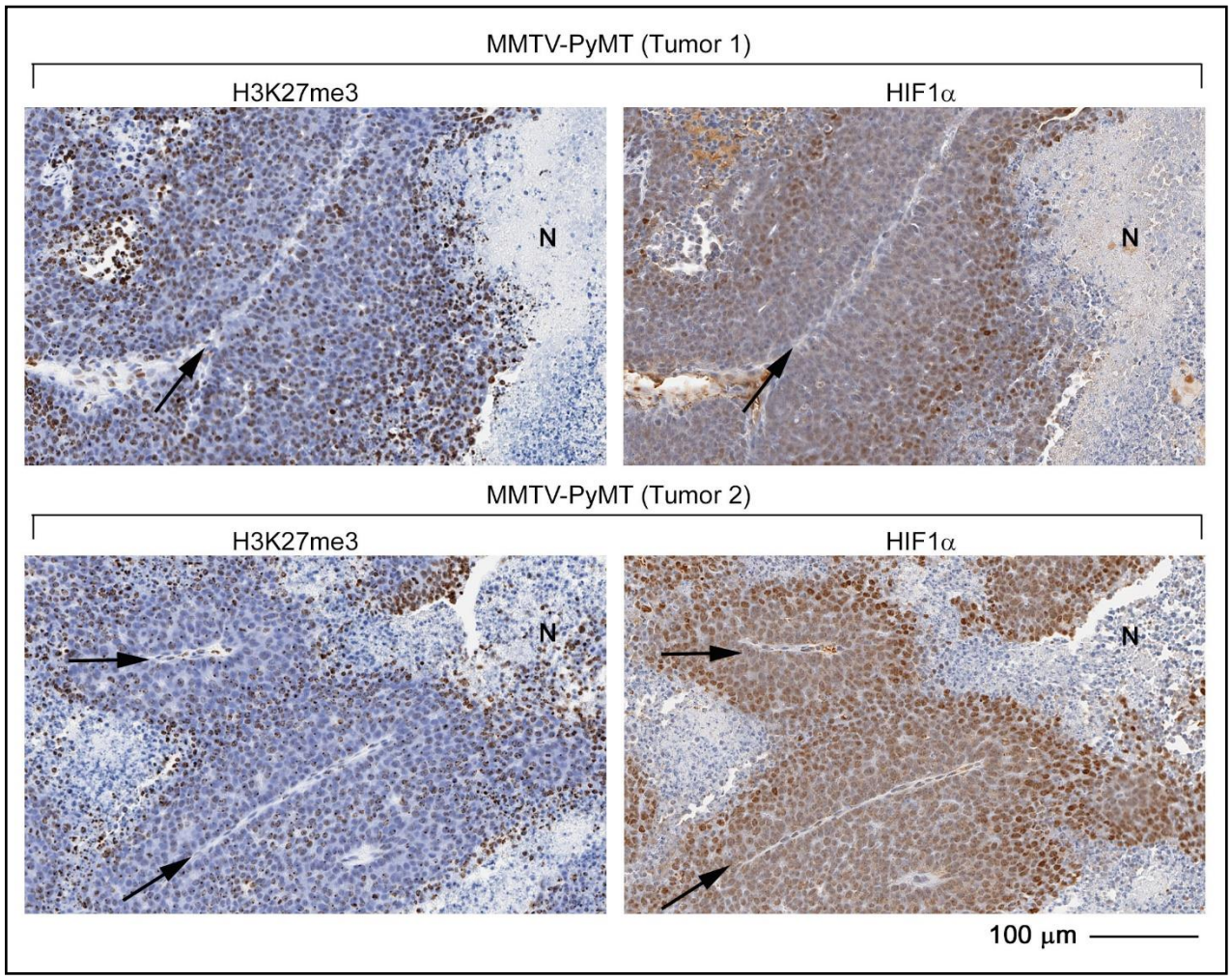

Fig. S10. Tumor Hypoxia Promotes Histone Hypermethylation.

Immunohistochemical analysis to compare localization of histone H3K27me3 and HIF1α, as indicated, in two independent breast tumors harvested from transgenic mice expressing mouse mammary tumor virus LTR-driven Polyoma virus middle T antigen [MMTV-PyMT. Blood vessel lumens are indicated by the arrows. Images are representative from analysis of 5 independent tumors.

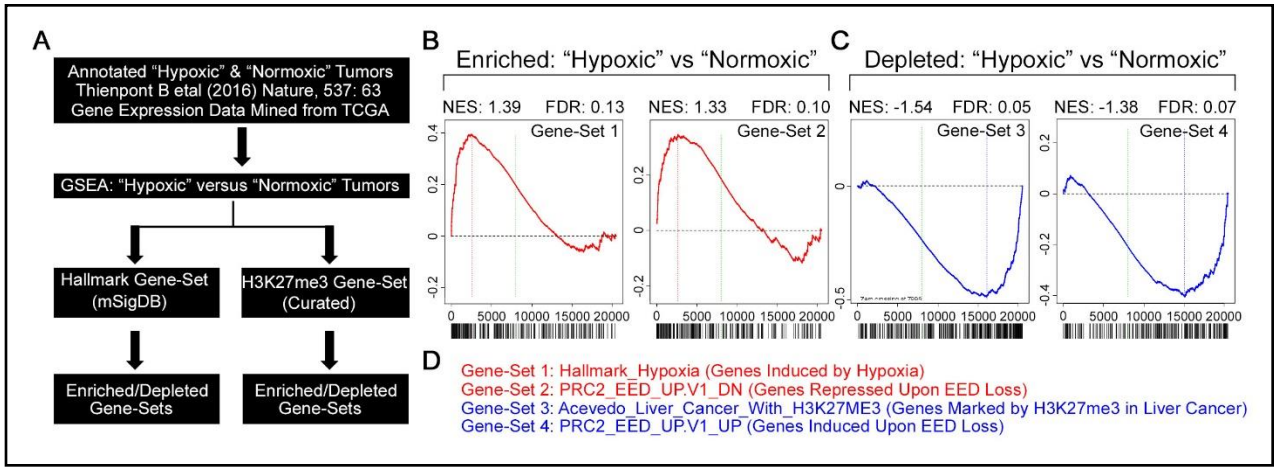

Fig. S11. Hypoxic Tumors Display a Transcriptional Signature Consistent with H3K27 Hypermethylation.

(**A**-**D**) Analytical flowchart (**A**) and Gene Set Enrichment Analysis showing the enrichment plots for transcriptional signatures that are enriched (**B**) or depleted (**C**) in "hypoxic" tumors. (**D**) Description of gene sets shown in (**B**) and (**C**).

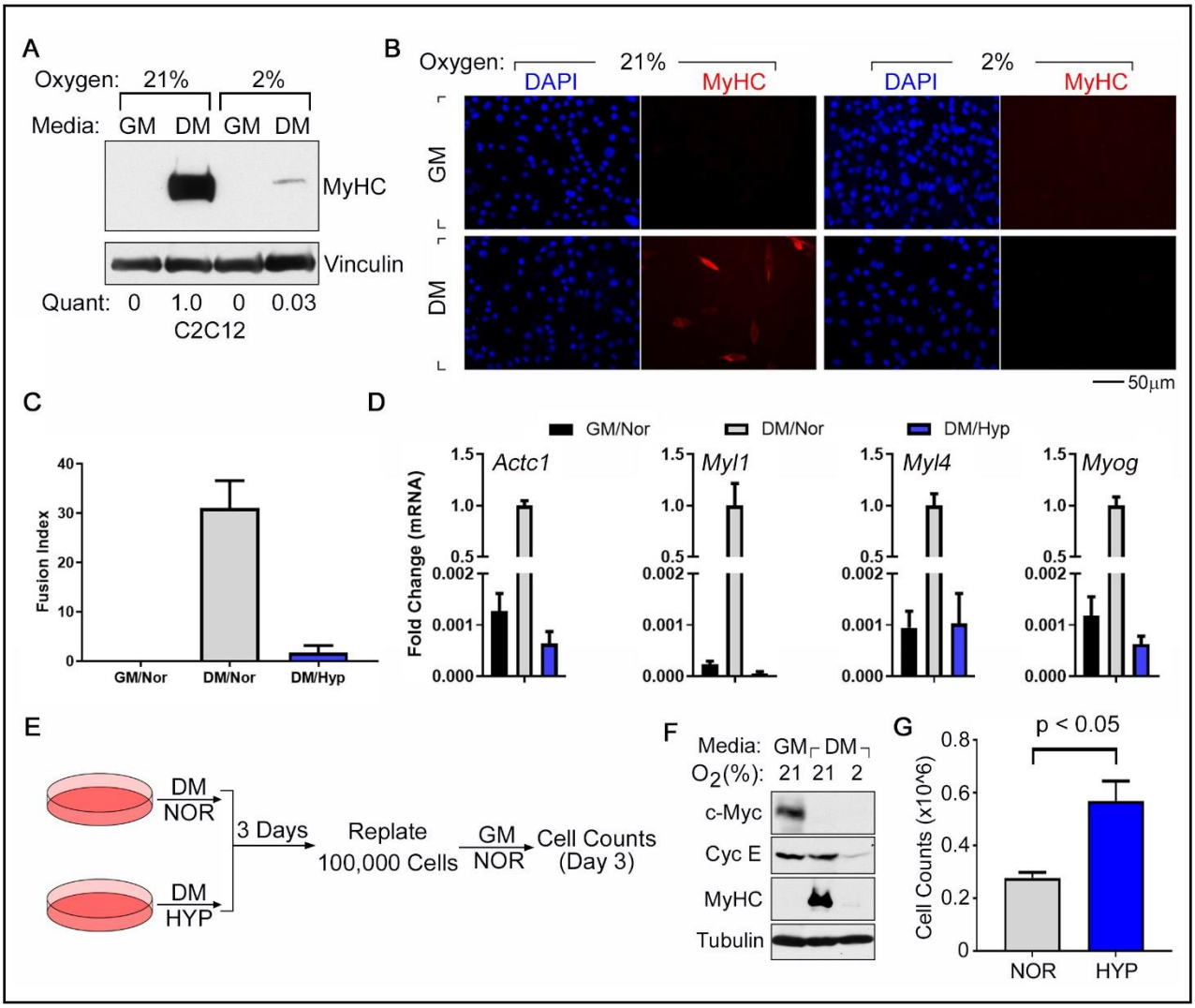

Fig. S12. Hypoxia Blocks Differentiation by Arresting Cells in a Reversible Quiescence-like State.

(**A**-**D**) Immunoblot analysis (**A**), Immunofluorescence analysis (**B**), fusion index measurements (**C**) or Real-Time qPCR analysis to measure the mRNA levels of the indicated myogenic markers (**D**) in C2C12 cells that were cultured either at 21% (nor) or 2% oxygen (hyp) in the indicated media for 4 days. (**E**) Schema for testing the ability of C2C12 cells to proliferate after

growth in DM under hypoxic conditions. (**F**) Immunoblot analysis of C2C12 cells after growth in DM under hypoxia or normoxia for 3 days, prior to replating as in (**E**). (**G**) Cell counts of viable C2C12 cells measured after replating in growth medium under normoxic conditions for 3 days as in (**E**). Data in (**C**), (**D**), and (**G**) represent mean +/- SD (*N*=3). In (**A**), "Quant" represents fold-change in densitometric ratios of MyHC (normalized to Vinculin) relative to normoxic cells cultured to DM.

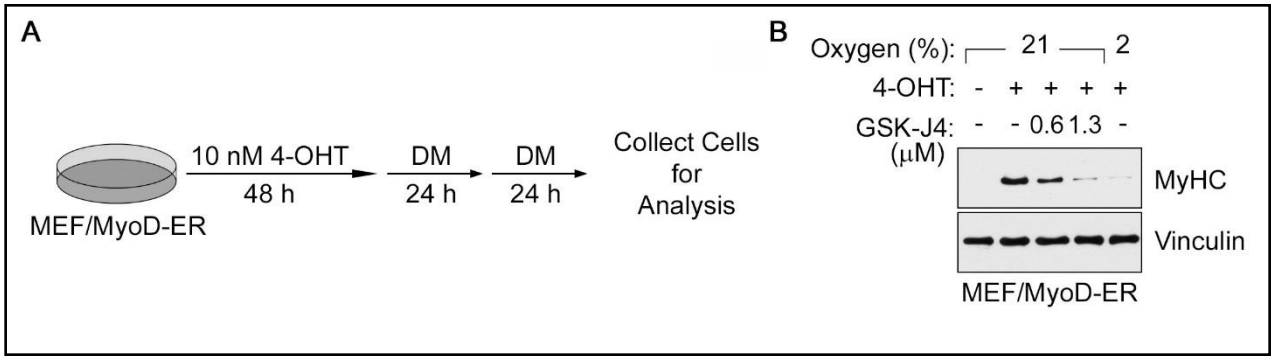

Fig. S13. Hypoxia Blocks Myogenic Differentiation in MyoD-ER Expressing Mouse Embryonic Fibroblasts

(**A**-**B**) Experimental Scheme (**A**) and Immunoblot Analysis (**B**) of Mouse Embryonic Fibroblasts that were lentivirally transduced to express MyoD-ER, as previously described (*39*). In (**B**) cells were induced to differentiate as in (**A**) at the indicated oxygen concentrations in the presence or absence of GSK-J4. [4OHT = 4-Hydroxy Tamoxifen].

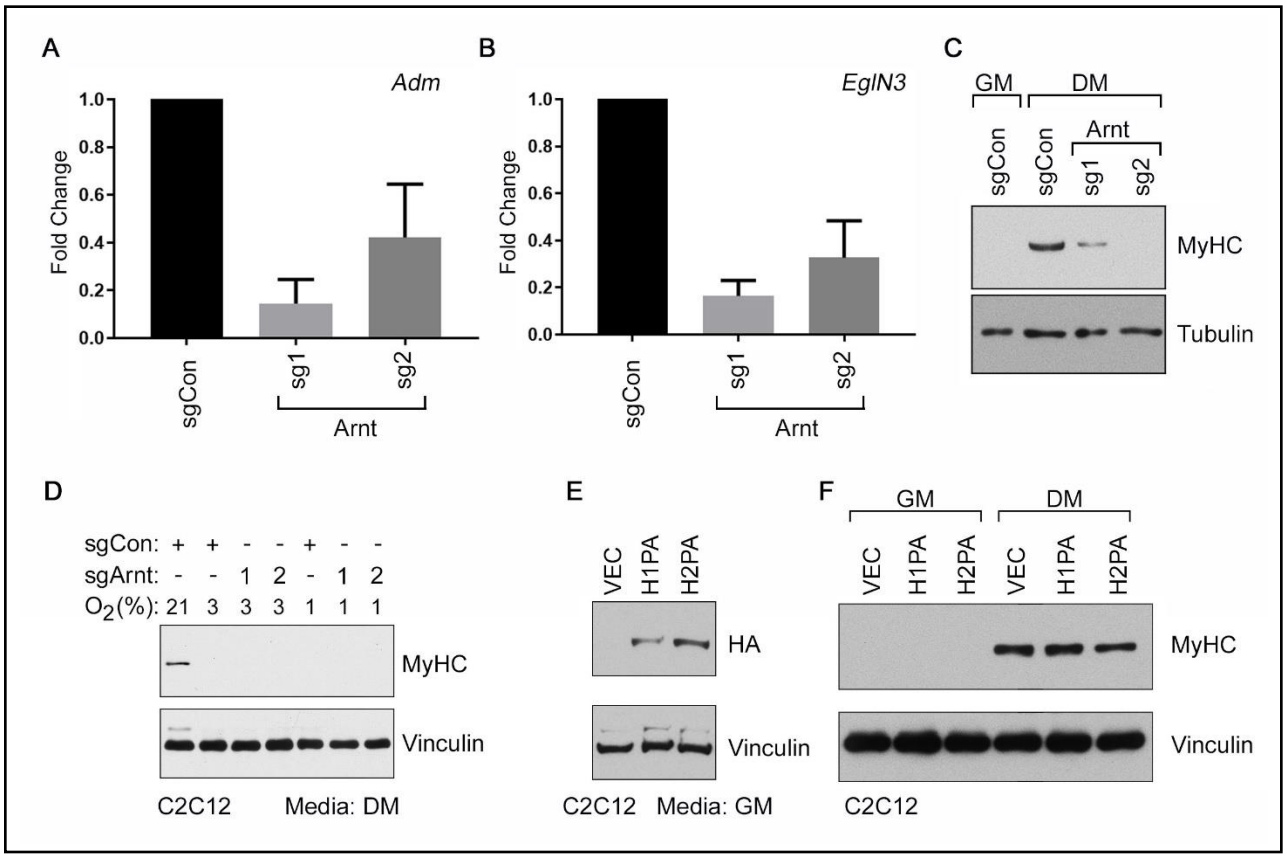

Fig. S14. HIF Activity is Necessary for Differentiation and Not Sufficient to Block Differentiation of C2C12 Myoblasts.

(**A**-**D**) Real-Time qPCR analysis of *Adm* (**A**) and *Egln3* (**B**) mRNAs and immunoblot analysis (**C** and **D**) of C2C12 cells that were lentivirally transduced to express the indicated sgRNAs targeting ARNT (ARNT sg1 and sg2) or a non-targeting control (sgCon) in the presence of Cas9. In (**A**) and (**B**) cells were cultured in growth medium at 2% oxygen for 24 hours and data represents mean +/- SD (*N*=3). In (**C**) cells were cultured either in growth medium [GM] or differentiation medium [DM], as indicated, in 21% oxygen for 4 days. In (**D**) cells were cultured in DM at the indicated oxygen concentrations for 4 days. (**E**-**F**) Immunoblot analysis of C2C12

cells that were lentivirally transduced to produced HA-tagged versions of mutant HIF1α [H1PA], mutant HIF2α [H2PA], or empty vector [VEC] as a control. In (**E**) cells were seeded in GM and harvested after 24 hours. In (**F**) cells were cultured in the indicated media in 21% oxygen for 4 days. The H1PA and H2PA variants contain alanine residues in place of the prolyl residues that are normally hydroxylated by the EglN prolyl hydroxylases, as described in (*55*).

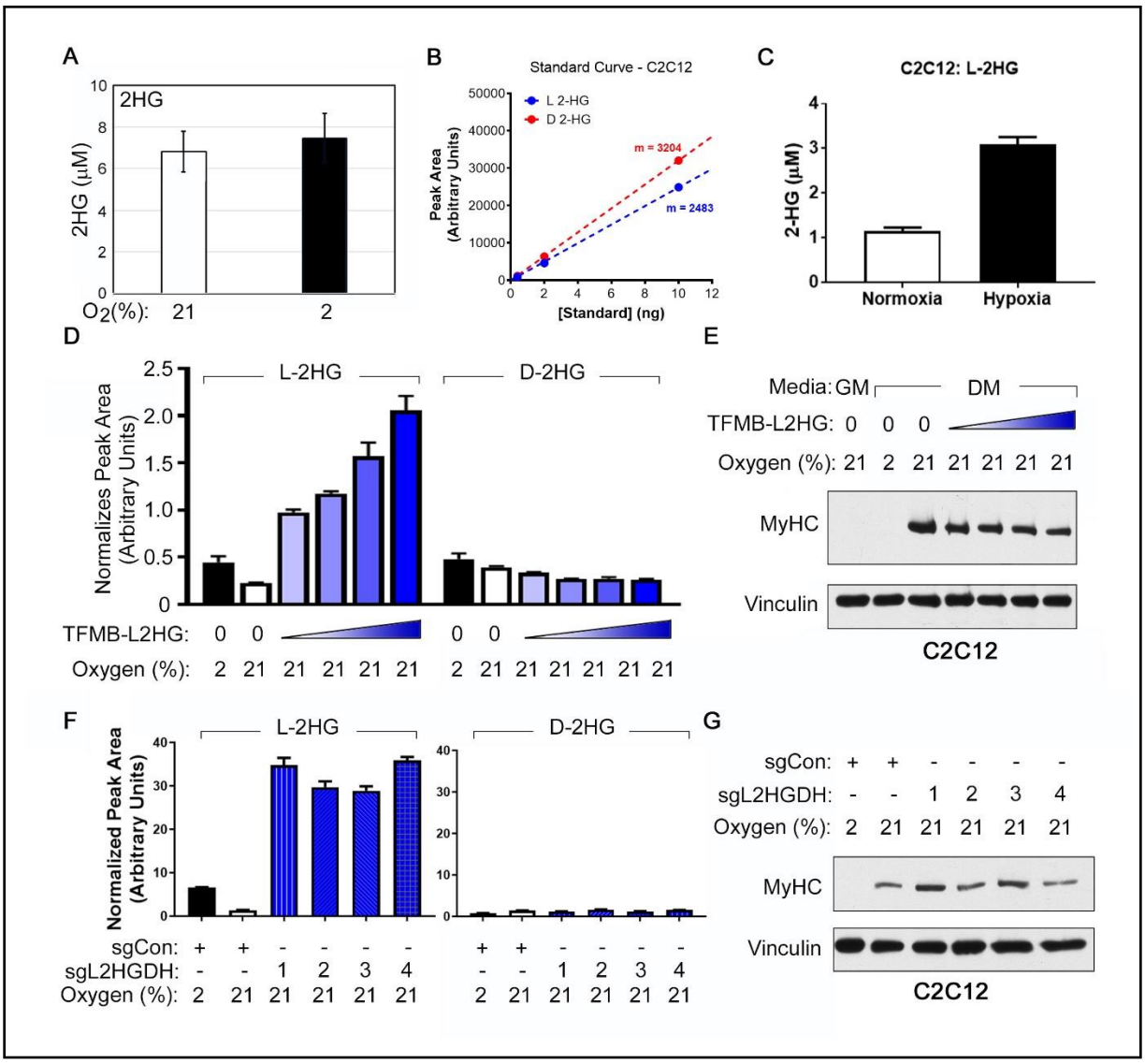

Fig. S15. Hypoxic L-2HG Production is Not Sufficient to Block Differentiation in C2C12 Myoblasts.

(**A**) Intracellular total 2HG levels in C2C12 cells determined by GC-MS, measured against a 2HG standard curve in water. (**B**-**C**) Intracellular L-2HG levels in C2C12 cells determined by LC-MS. Peak areas determined using a standard curve of $^{13}C_5$-2-HG in C2C12 cell matrix (**B**) were used to measure absolute intracellular concentrations of L-2HG (**C**) in C2C12 cells that

were cultured for 4 days in differentiation media at either 21% oxygen (Normoxia) or 2% oxygen (Hypoxia). (**D)** Intracellular enantiomer-specific 2-HG levels, normalized to the spiked-in $^{13}C_5$-2-HG internal standard, as determined by LC-MS. Triangles indicate treatment with a 3-fold serial dilution range (19, 56, 167, and 500 μM) of an esterified (TFMB) version of L-HG**.** Esterified L-2HG was replenished at every daily media change and measurements were made 3 hours after the last media change. (**E**) Immunoblot analysis of C2C12 cells treated with TFMB-L2HG as in (**D**) in the indicated media and oxygen environments. (**F**) Intracellular enantiomer-specific 2-HG levels, normalized to the spiked-in $^{13}C_5$-2-HG internal standard, as determined by LC-MS, in C2C12 cells that were lentivirally transduced to express the indicated L2HGDH (sgL2HGDH) sgRNAs or control (sgCon) and cultured at the indicated oxygen concentrations in differentiation media for 4 days. (**G**). Immunoblot analysis of C2C12 cells as in (**F**) grown in DM at the indicated oxygen concentrations. Data in (**A**), (**C**), (**D**), and (**F**) represent mean +/- SD (*N*=3).

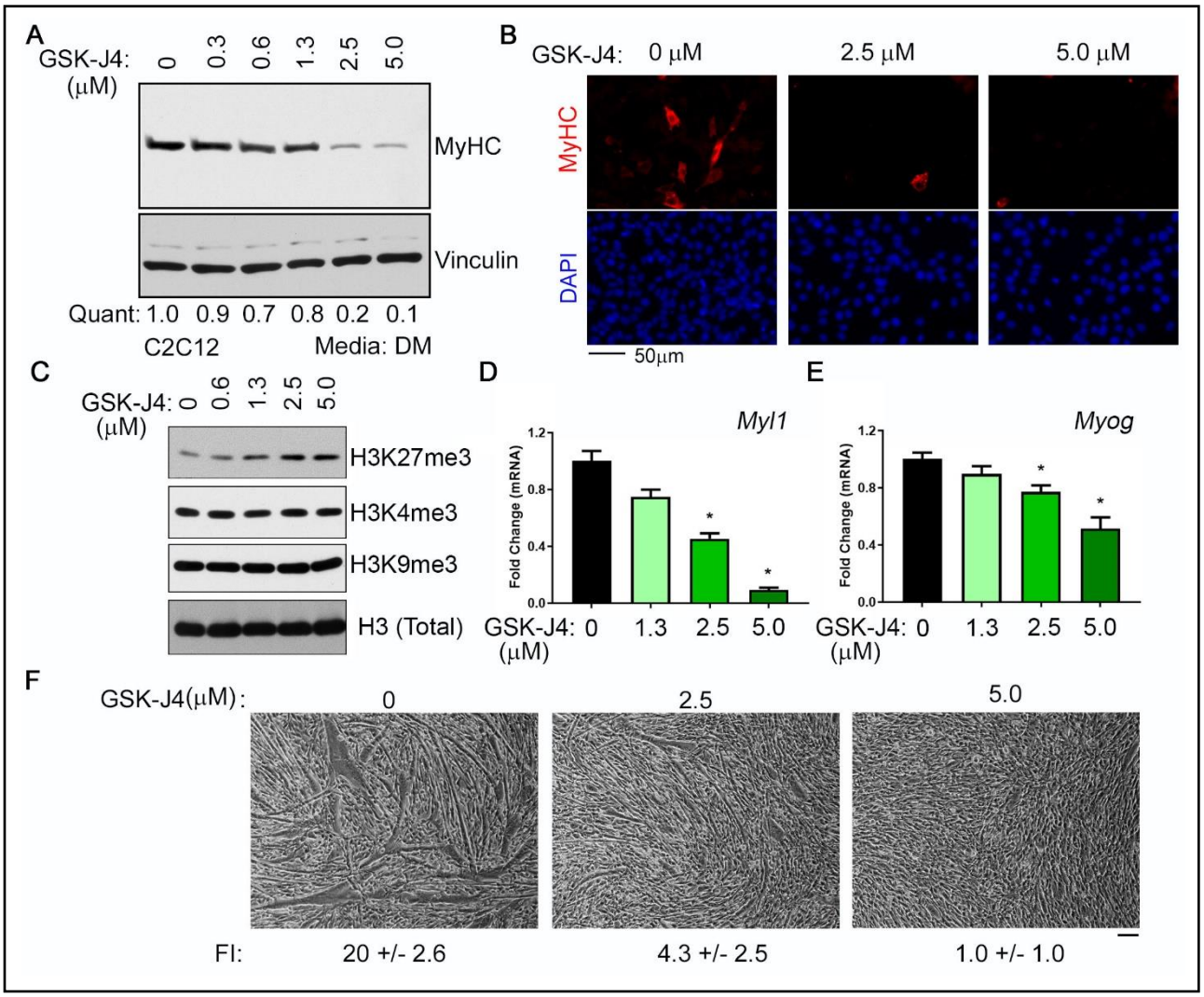

Fig. S16. Treatment with GSK-J4 Blocks Differentiation in C2C12 Myoblasts.

(**A**-**C**) Immunoblot analysis of whole cell lysates (**A**), Immunofluorescence Analysis (**B**), and Immunoblot analysis of histone lysates (**C**), of C2C12 cells treated with the indicated concentrations of GSK-J4 for 3 days in DM. (**D**-**F**) Fold change in mRNA levels (normalized to *Actin*) of *Myl1* (**D**) and *Myog* (**E**), as measured by Real-Time qPCR, and Photomicrographs (**F**) of C2C12 cells that were cultured in differentiation media in the presence of the indicated concentrations of GSK-J4 for 4 days. In (**A**), "Quant" represents fold-change in densitometric

ratios of MyHC (normalized to Vinculin) relative to normoxic cells cultured to DM. In (**D**) and (**E**), data represents mean +/- SD (*N*=3) and [*] represents $p<0.05$ calculated by Students *t-test*. In (**F**), Fusion Index (FI) is represented as mean +/- SD (*N*=3), and scalebar represents 200 µm.

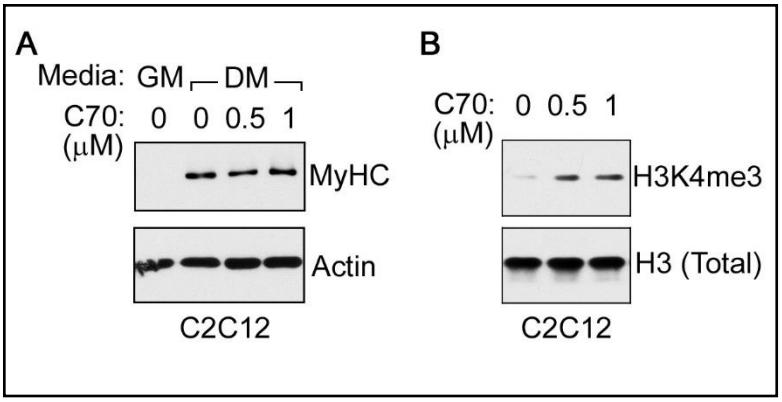

Fig. S17. Treatment with KDM-C70 Does Not Block the Differentiation of C2C12 Myoblasts.

(**A**-**B**) Immunoblot analysis of soluble protein (**A**) and histone lysates (**B**) generated from C2C12 cells cultured in the indicated media in (**A**) or in DM in (**B**) in the presence of the indicated concentrations of KDM-C70 for 4 days.

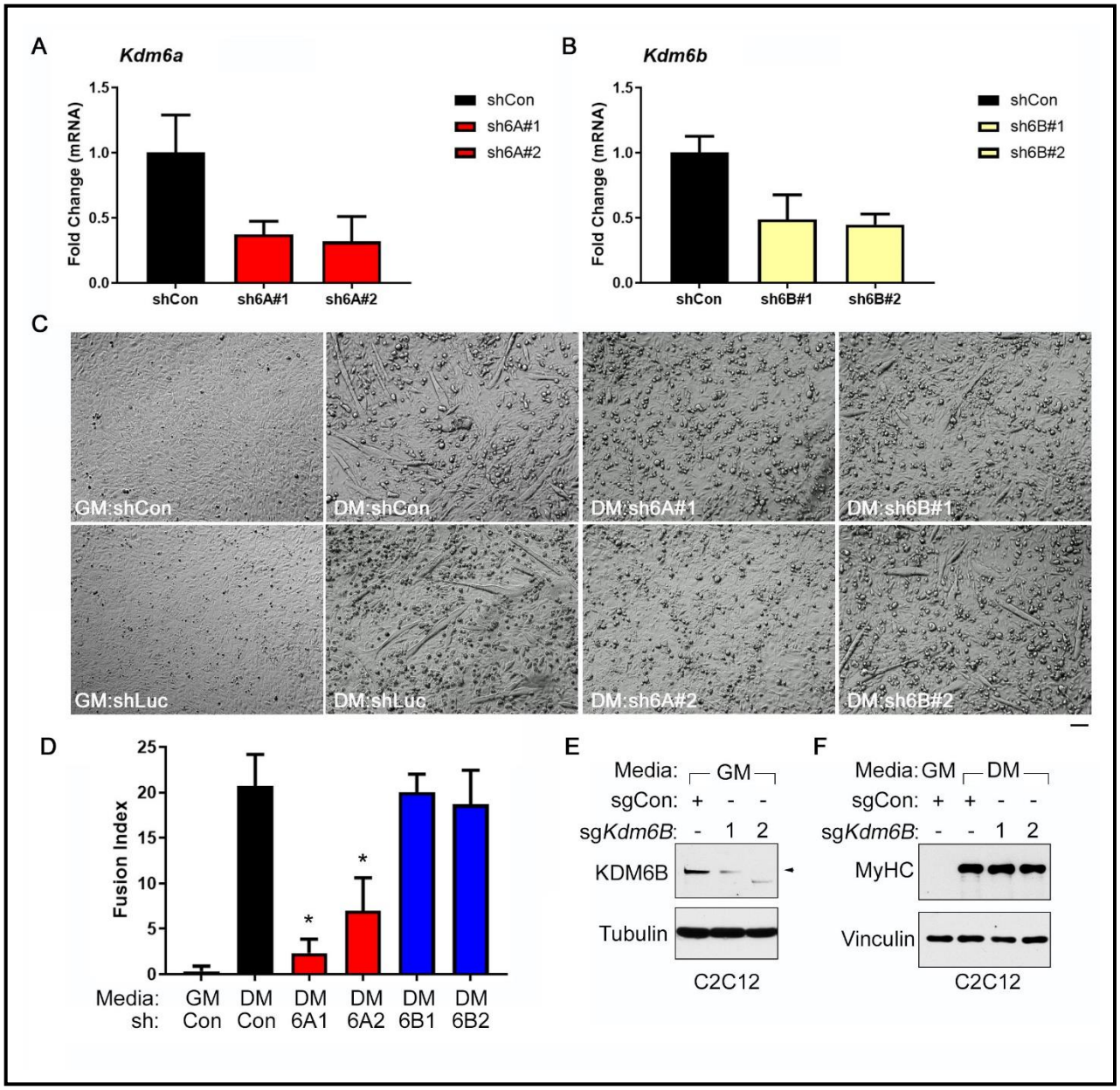

Fig. S18. KDM6B Inactivation Does Not Block Differentiation in C2C12 Myoblasts.

(**A**-**B**) Real-Time qPCR analysis to measure *Kdm6A* (**A**) and *Kdm6B* (**B**) mRNAs in C2C12 cells that were lentivirally transduced to express short-hairpin RNAs targeting *Kdm6A* [sh6A#1 and sh6A#2], *Kdm6B* [sh6B#1 and sh6B#2], or a non-targeting control shRNA [shCon]. Data represent mean +/- SD (*N*=3). (**C**-**D**) Photomicrographs (**C**) and Fusion Index Measurements (**D**)

of C2C12 cells that were lentivirally transduced to express the indicated shRNAs and then cultured in the indicated media for 4 days. In (**C**) scalebar represents 200 µm. In (**D**), data represent mean +/- SD (*N*=3), and [*] indicates $p<0.05$ calculated by Students *t-test*. (**E**-**F**) Immunoblot analysis from C2C12 cells lentivirally transduced to express *Kdm6B* sgRNA or control (Con) sgRNA. In (**E**) cells cultured in the indicated media were analyzed 7 days post infection. In (**F**) cells were cultured in the indicated media for 4 days.

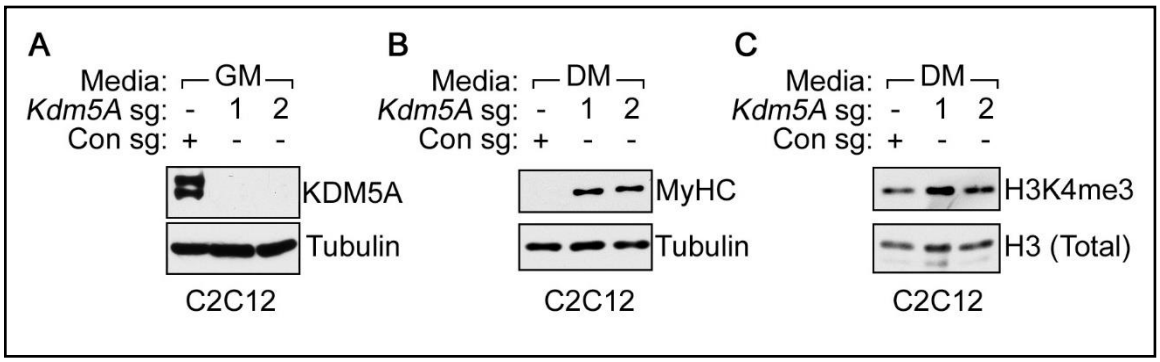

Fig. S19. KDM5A Inactivation Promotes Myogenic Differentiation in C2C12 Cells.

(**A**-**C**) Immunoblot analysis of soluble proteins (**A** and **B**) and histone lysates (**C**) from C2C12 cells that were lentivirally transduced to express the indicated *Kdm5A* sgRNAs or control (Con) sgRNA. In (**A**) cells cultured in the indicated media were analyzed 7 days post infection. In (**B**) and (**C**) cells were cultured in the indicated media for 4 days. Note that in panel (**B**) the absence of a MyHC signal in lane 1 is because it was necessary to do a very short exposure due to the strong MyHC signal in lanes 2 and 3.

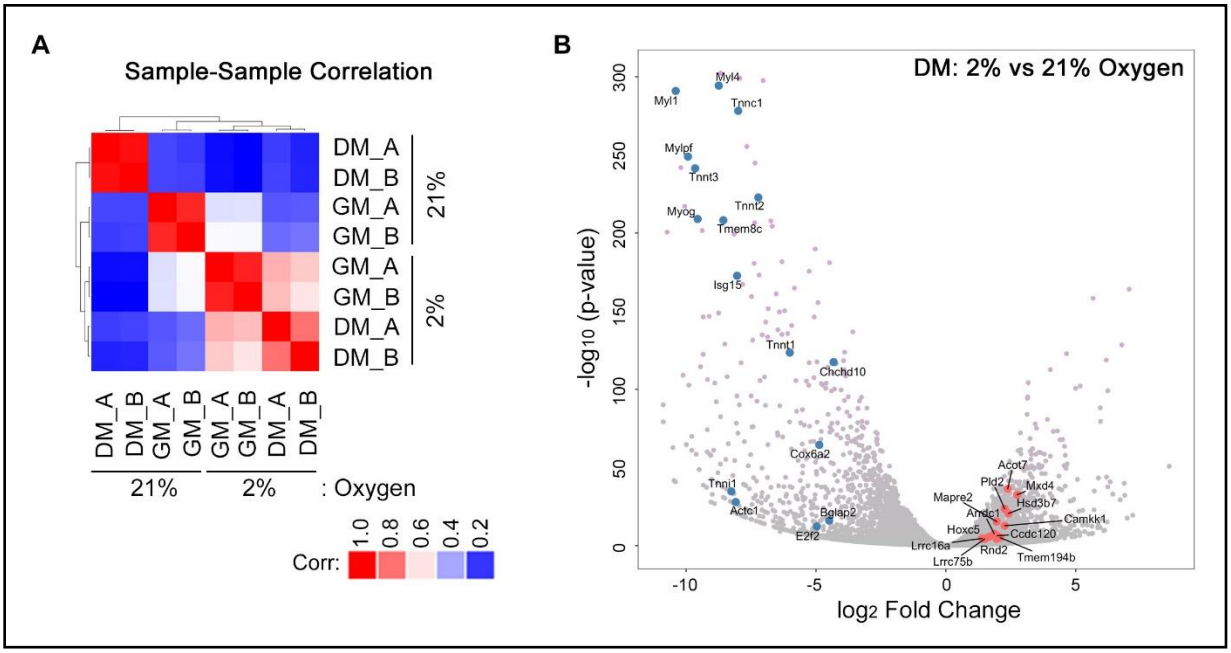

Fig. S20. Hypoxia Imposes a Transcriptional Block on Myogenic Regulators in Differentiating C2C12 Cells.

(A-B) Pearson correlation (**A**) and Volcano Plot (**B**) of mRNA expression levels determined by RNA-seq from two biological replicates (A and B) of C2C12 cells cultured in growth media (GM) or differentiation media (DM), as indicated, for 4 days at the indicated oxygen concentration.

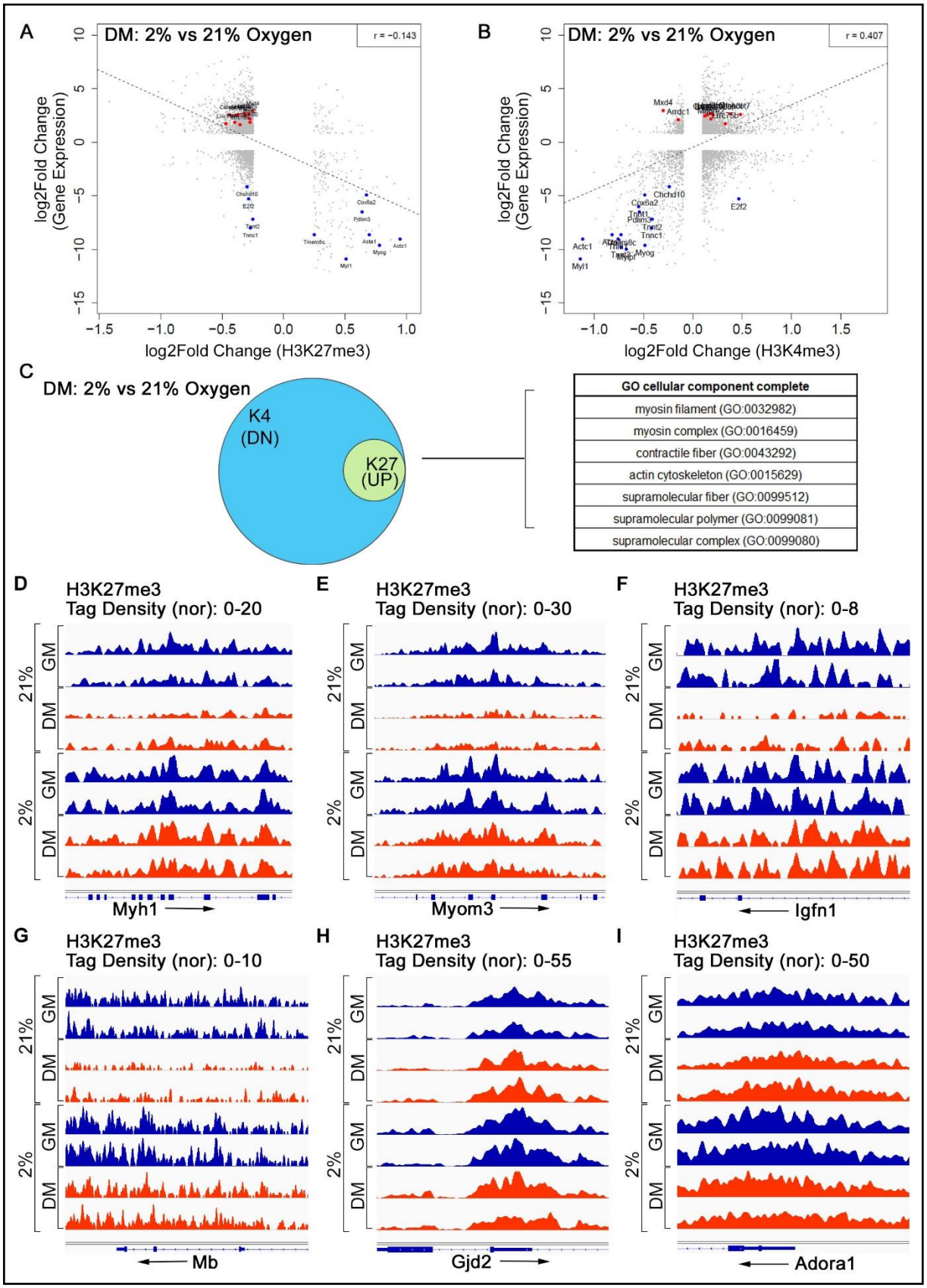
A
DM: 2% vs 21% Oxygen
r = −0.143
log2Fold Change (Gene Expression)
log2Fold Change (H3K27me3)
B
DM: 2% vs 21% Oxygen
r = 0.407
log2Fold Change (Gene Expression)
log2Fold Change (H3K4me3)
C
DM: 2% vs 21% Oxygen
K4 (DN)
K27 (UP)
GO cellular component complete
myosin filament (GO:0032982)
myosin complex (GO:0016459)
contractile fiber (GO:0043292)
actin cytoskeleton (GO:0015629)
supramolecular fiber (GO:0099512)
supramolecular polymer (GO:0099081)
supramolecular complex (GO:0099080)
D
H3K27me3
Tag Density (nor): 0-20
Myh1
E
H3K27me3
Tag Density (nor): 0-30
Myom3
F
H3K27me3
Tag Density (nor): 0-8
Igfn1
G
H3K27me3
Tag Density (nor): 0-10
Mb
H
H3K27me3
Tag Density (nor): 0-55
Gjd2
I
H3K27me3
Tag Density (nor): 0-50
Adora1
21%
2%
GM
DM

Fig. S21. Genomic Analysis Demonstrates Failure to Erase H3K27me3 at Myogenic Regulators in Hypoxic C2C12 Cells.

(**A**-**C**) Correlation of genomic recruitment (as measured by ChIP-Seq) versus gene expression (as measured by RNA-Seq) for H3K27me3 (**A**) and H3K4me3 (**B**) in C2C12 cells that were cultured in differentiation media (DM) at either 21% or 2% oxygen. Gene Ontology Enrichment in (**C**) comparing biological processes that show increased recruitment of H3K27me3 and decreased recruitment of H3K4me3 in hypoxic (2%) versus normoxic (21%) cells. (**D**-**I**) H3K27me3 recruitment, as measured by tag density from ChIP-Seq data, in C2C12 cultured under the indicated conditions for 4 days. Recruitment at the myogenic markers *Myh1* (**D**), *Myom3* (**E**), *Igfn1* (**F**), and *Mb* (**G**) [and *Actc1*, *Myl1*, and *Myog* shown in Fig. 2, **H** to **J**]. *Gjd2*, which lies adjacent to *Actc1*; and *Adora1*, which lies adjacent to *Myog*; were included as specificity controls.

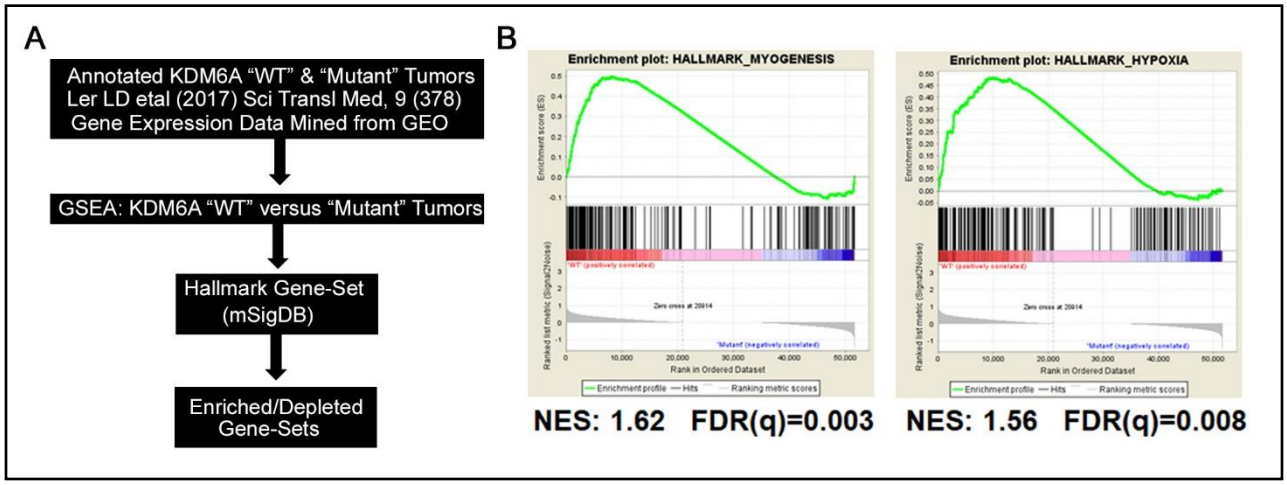

Fig. S22. KDM6A Loss is Associated with Hallmarks of Dedifferentiation in Bladder Tumors

(**A**-**B**) Analytical flowchart (**A**) and Gene Set Enrichment Analysis showing the enrichment plots for transcriptional signatures that are enriched in KDM6A wild-type "WT" versus KDM6A "Mutant" tumors (n=10 in each group). Note that the wild-type KDM6A tumors have increased expression of "Hallmark Myogenesis" mRNAs relative to KDM6A mutant tumors. This does not appear to be because the KDM6A mutant tumors are more hypoxic if one examines levels of "Hallmark Hypoxia" mRNAs, which are actually higher in the wild-type KDM6A tumors. FDR (q) values below 0.25 were considered statistically significant.

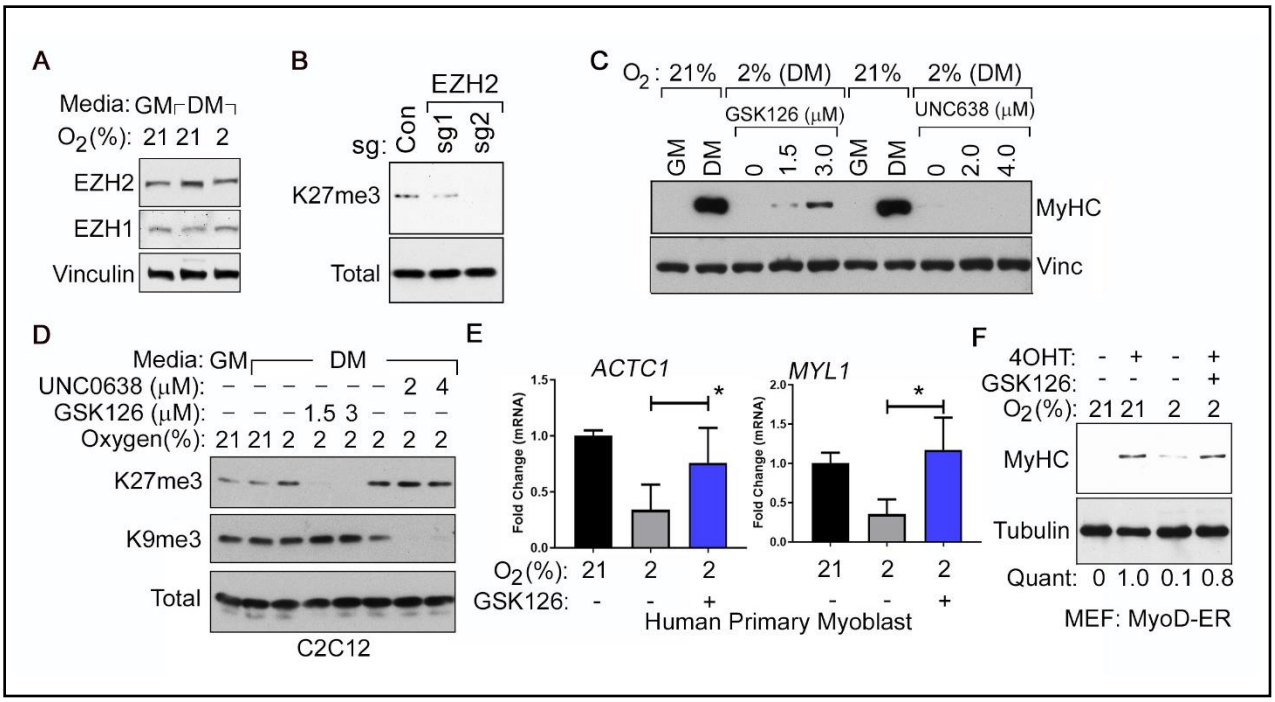

Fig. S23. Pharmacological Inhibition of EZH2 Rescues the Hypoxic Differentiation Block in Myogenic Cells

(**A)** Immunoblot analysis of C2C12 myoblasts cultured in the indicated media and oxygen concentrations for 2 days. (**B**) Immunoblot analysis of histone lysates prepared from C2C12 myoblasts that were transduced to express either *Ezh2* sgRNAs or a control (Con) sgRNA, as indicated. Histones were extracted 7 days post infection. (**C**-**D**) Immunoblot analysis of whole cell lysates (**C**) and of histone lysates (**D**) generated from C2C12 cells treated with the indicated concentrations of GSK126 or UNC0638 for 4 days. Cells were cultured either in 21% oxygen (NOR) or 2% oxygen (HYP) in growth medium (GM) or differentiation medium (DM), as indicated. (**E**) mRNA levels of myogenic differentiation markers, relative to Actin mRNA, measured by Real-Time qPCR of RNA obtained from primary human skeletal myoblasts that

were cultured in differentiation media at the indicated oxygen concentrations in the presence or absence of 2 μM GSK126, as indicated. Data represent mean +/- SD (*N*=3), and [*] indicates $p<0.05$ calculated by Students *t-test*. (**E**) Immunoblot analysis of MyoD-ER expressing Mouse Embryonic Fibroblasts, described in fig. S13 and (*39*), cultured in differentiation media under the indicated oxygen concentrations in the presence or absence of 2 μM GSK126, as indicated. "Quant" represents fold-change in densitometric ratios of MyHC (normalized to Tubulin) relative to normoxic cells treated with 4-OHT. [4OHT=4-Hydroxy Tamoxifen].

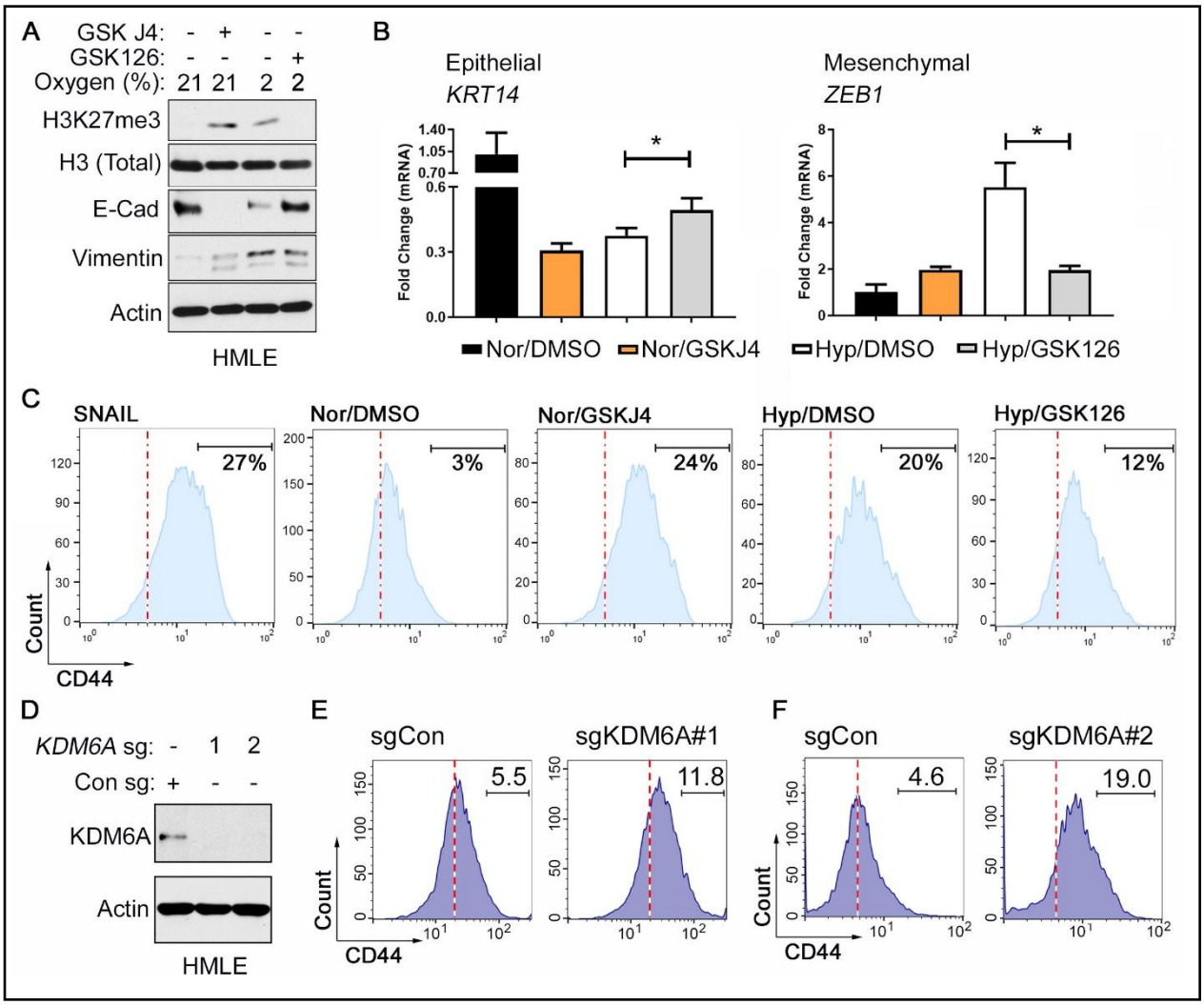

Fig. S24. Modulating H3K27me3 Regulates EMT in Human Mammary Epithelial (HMLE) Cells

(**A**-**C**) Immunoblot Analysis (**A**), mRNA levels of EMT markers (relative to Actin) determined by Real-time qPCR analysis (**B**), and flow cytometric analysis (**C**), of HMLE cells that were cultured at 21% Oxygen (Nor) or 2% Oxygen (Hyp) for 7 days in the presence 2 μM GSK-J4, 3 μM GSK126, or DMSO as indicated. In (**C**), SNAIL represents data from HMLE cells lentivirally transduced to express the transcription factor SNAIL, a master regulator of EMT. (**D**-**F**) Immunoblot analysis (**D**) and flow cytometric analysis (**E** and **F**) of HMLE cells that were

lentivirally transduced to express one of two different *KDM6A* sgRNAs or a control sgRNA and cultured under normoxic conditions for 7 days post selection. Data in (**B**) represent mean +/- SD (*N*=3). (**C**), (**E**), and (**F**) is representative of 3 independent experiments.

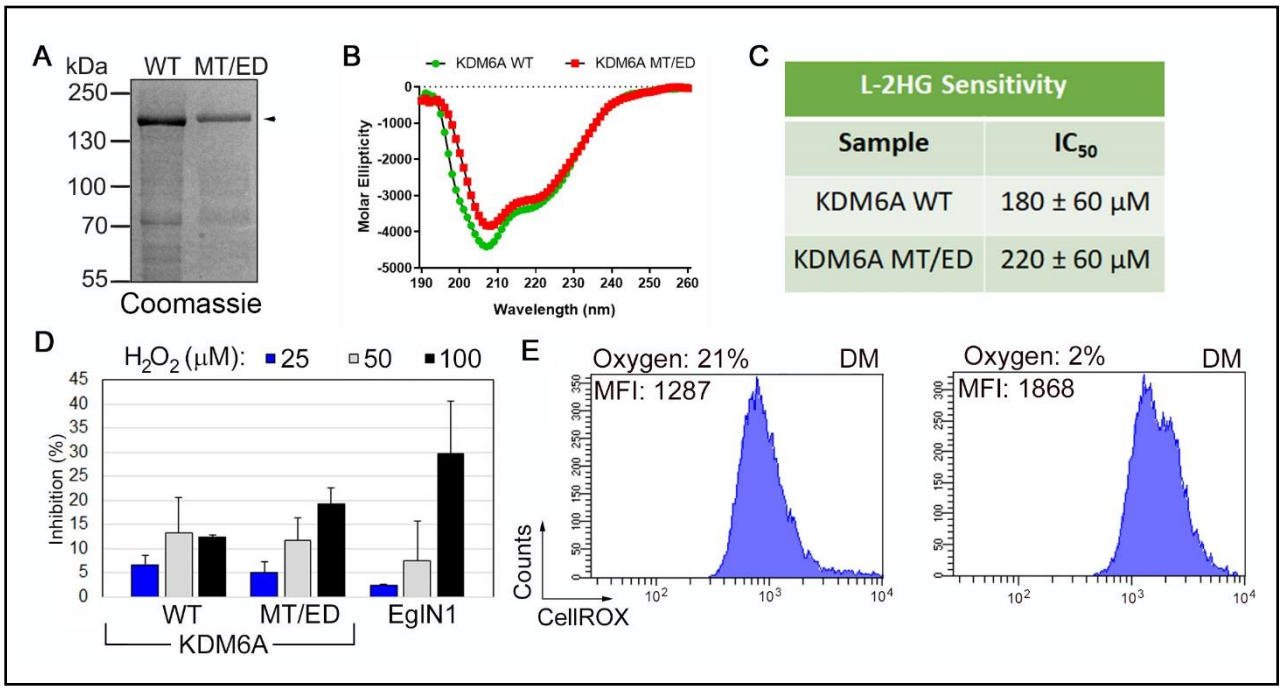

Fig. S25. Wild-Type and Mutant KDM6A are Equally Insensitive to L-2HG and ROS

(A-B) Coomassie blue staining (**A**), Circular Dichroism analysis (**B**), and IC_{50} values of L-2HG determined *in vitro* (**C**) using recombinant wild-type KDM6A or the MT/ED mutant. (**D**) Percent inhibition in activity of the indicated proteins upon exogenous addition of the indicated concentrations of H_2O_2 (25 or 50 µM). Inhibition was calculated as a percentage loss in activity compared to reactions not containing H_2O_2. (**E**) Intracellular ROS levels as measured by flow cytometry after CellROX staining in C2C12 cells that were cultured in differentiation media (DM) at the indicated oxygen concentrations for 3 days. In (**C**) and (**D**), data represent mean +/- SD (*N*=3). In (**E**), data is representative of 3 independent measurements. [MFI = Mean Fluorescence Index].

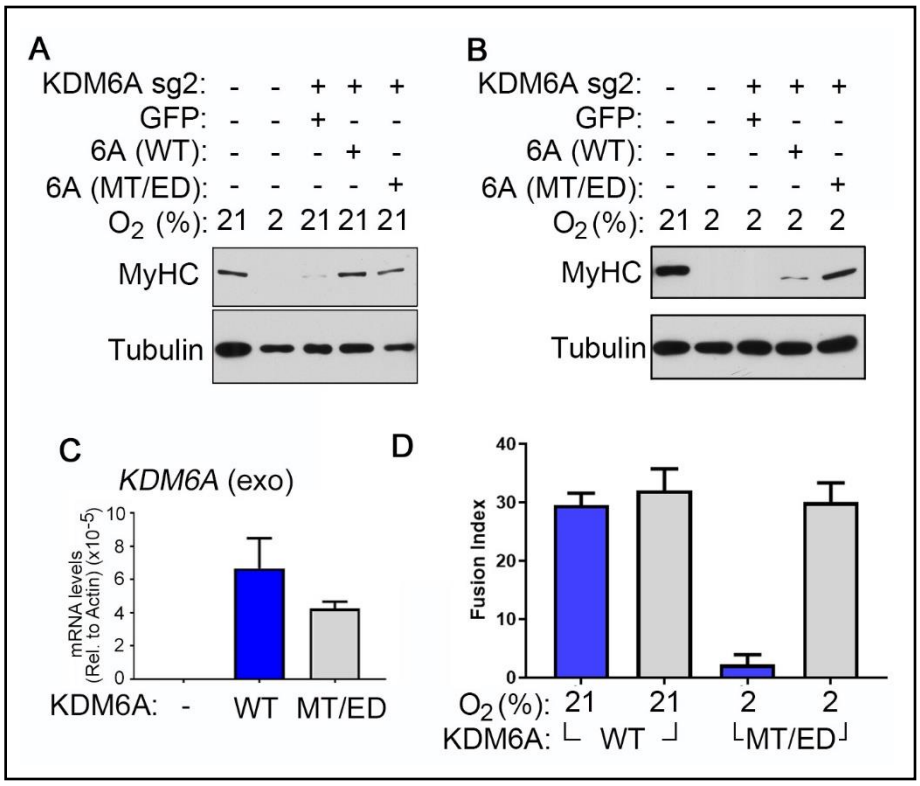

Fig. S26. Reintroduction of an Enhanced Oxygen Affinity KDM6A Mutant is Sufficient to Rescue the Hypoxic Differentiation Block in C2C12 Cells

(**A**-**B**) Immunoblot analysis of C2C12 cells expressing, where indicated, *Kdm6a* sg2 [described in Fig. 2, (**C**) and (**D**)] that were lentivirally transduced to produce wild-type human KDM6A [6A(WT)], the human KDM6A MT/ED double mutant [6A(MT/ED)], or GFP (control), and then cultured in differentiation media at the indicated oxygen concentrations for 4 days. (**C-D**) Real-Time qPCR analysis (**C**) and Fusion Index measurements (**D**) for cells described in Fig. 3, (**F**) and (**G**). Data represent mean +/- SD (*N*=3).